MECHANICAL AND ELECTRONIC PROPERTIES OF METAL CHAIN NANOWIRES

A THESIS

SUBMITTED TO THE DEPARTMENT OF PHYSICS

AND THE INSTITUTE OF ENGINEERING AND SCIENCE

OF BILKENT UNIVERSITY

IN PARTIAL FULFILLMENT OF THE REQUIREMENTS

FOR THE DEGREE OF

MASTER OF SCIENCE

By

Deniz Çakır

August, 2003

I certify that I have read this thesis and that in my opinion it is fully adequate, in scope and in quality, as a thesis for the degree of Master of Science.

Assist. Prof. Dr. Oğuz Gülseren (Supervisor)

I certify that I have read this thesis and that in my opinion it is fully adequate, in scope and in quality, as a thesis for the degree of Master of Science.

Prof. Dr. Bilal Tanatar

I certify that I have read this thesis and that in my opinion it is fully adequate, in scope and in quality, as a thesis for the degree of Master of Science.

Dr. Taner Yıldırım

Approved for the Institute of Engineering and Science:

Prof. Dr. Mehmet B. Baray
Director of the Institute Engineering and Science

ABSTRACT

MECHANICAL AND ELECTRONIC PROPERTIES OF METAL CHAIN NANOWIRES

Deniz Çakır
M.S. in Physics
Supervisor: Assist. Prof. Dr. Oğuz Gülseren
August, 2003

The fabrication of stable gold monoatomic chains suspended between two gold electrodes is one of the milestones in nanoscience and technology, since miniaturization of the electronic components is one of the great importance in development and improvement of new devices in nanoelectronic. Monoatomic chain nanowires show unusual mechanical and electronic properties such as quantized conductance and much stiff bonds compare to the ones in bulk. Ohnishi *et al.* [1], has visualized the monoatomic chains by using transmission electron microscopy (TEM). At the same time, Yanson *et al* [2], have produced the monoatomic chains and they measured its conductance. In the bond length measurement of monoatomic chains, unusually long interatomic lengths have been observed compare to interatomic distances in the bulk and dimer. In order to understand the nature of bonding and unusual structural properties, in this thesis, mechanical and electronic properties of metal chain nanowires are investigated from first principles by using pseudopotential plane wave calculations. Six different metals (Au, Ag, Al, Cu, Pt and Na) are studied in detail. All metals under study show two wire structure which are linear and zigzag structure. Au, Al and Pt show two different zigzag structure. All the wires are metallic. Relative stabilities are investigated by calculating the tension corresponding to apply force to keep the wire at a specific length. Au and Pt have bigger breaking force at breaking point relative to other metallic wires. In this thesis, effect of H, H_2 and C impurities on mechanical and electronic properties of Au monoatomic chains are also studied. In wires with H and C impurities, wire under tension break from Au-Au bond away from the impurity. However, wire break from Au-H bond in H_2 system. Except from Au-H system, wire become insulator when it contain C or H_2 impurities. Before breaking, Au-impurity-Au bond length is in the range of long interatomic distance observed in experiment. So, the presence of an impurity can explain the observed long interatomic distances. However, changing of bond lengths and

breaking bond during the stretching of wire depends on the type of impurity. If one stretch the Au-H system, all bond lengths increase in the same amount before breaking. However in Au-C system, Au-Au bond length away from the C impurity increase much more than other bonds. It is shown that absorption of impurity atoms modify the stiffness of the bonds in the wire. This related to the charge transfer from Au to impurity (for H and C). In H and C systems, wire break from Au-Au bond away from the impurity. However in H_2 system, wire break from Au-H bond.

Keywords: Nanowire, metal monatomic chains, mechanical and electronic properties, quantum conductance, impurity.

ÖZET

ATOMİK TELLERİN ELEKTRONİK VE MEKANİK ÖZELLİKLERİ

Deniz Çakır
Fizik , Yüksek Lisans
Tez Yöneticisi: Yar. Doç. Dr. Oğuz Gülseren
Ağustos, 2003

Boyutları küçültülmüş yeni aygıtların yapılmasına ve düşük boyutlardaki fiziksel özelliklerin incelenmesine olanak sağladığından dolayı tek atomlu altın tellerin yapılması nano-bilim ve teknoloji için çok önemli bir ilerlemedir. Nano teller ilk defa Ohnishi *et al.* [1], grubu tarafından transmisyon elektron mikroskopu (TEM) kullanılarak gözlendi. Aynı zamanlarda Yanson *et al.* [2], nano telleri yapmayı başardı ve elektriksel iletkenlik ölçümleri yaptı. Bu deneylerde çok büyük atomlar arası uzunluklar ölçüldü. Bu tezde ilk prensipler yöntemi kullanılarak metal nano tellerin mekanik ve elektronik özellikleri altı element (Au, Ag, Al, Cu, Pt ve Na) için incelendi. İncelenen elementler için dogrusal ve zigzag olmak üzere iki farklı tel geometrisi bulundu. Çalışılan tüm tek atomlu zincirlerin iletken oldukları bulundu. Ayrıca katkı atomlarının (H, C, H_2) altın tellerin elektronik ve mekanik özelliklerine olan etkileri incelendi. Au-H ve Au-C sistemlerinde tek atomlu zincir katkı atomun uzağındaki Au-Au bağından kırılmaktadır. Kırılmadan önce elde edilen Au-katkı atom-Au bağ uzunluğuna bakarsak deneylerde gözlenen büyük atomlar arası bağ uzunluklarına çok yakın sonuçlar elde edildi. Atomik tellerin çekilmesi sırasında bağ uzunluklarının değişimi ve kırılan bağ tellere eklenen katkı atomuna bağlı olduğu bulundu. Tellerin kırılmadan önceki uzunluklarına bakıldığında Au-H sisteminde bütün bağlar eşit oranda uzarken Au-C sisteminde C atomunun uzağındaki bağın diğerlerine göre daha çok uzadığı tespit edildi.

Anahtar sözcükler: Nano tel, tek atomlu metal zincir, mekanik ve elektronik özellikler, kuantum iletkenliği, katkı.

Acknowledgement

I would like to thank my supervisor Assist. Prof. Dr. Oğuz Gülseren, for support and encouragement.

I also would like to thank Sefa Dağ, Engin Durgun , Cem Sevik and Engin Emlek for their help in improving my knowledge about vasp and others subjects related to my thesis. But the important thing is their friendship.

Contents

List of Figures

List of Tables

Chapter 1

INTRODUCTION

In the last decade, there has been a great interest in both fabrication of nanowires and their mechanical, electrical and geometrical properties. Nanowires are important, since they show very interesting properties from a basic science viewpoint, as well as great potential in applied fields such as nanoelectronics. Nanoscale materials have peculiar properties different from crystalline structures due to the quantum confinement of electrons. In Ohm's law electrical resistance of a conductor is proportional to its length. However, this law breaks down at low dimensions. The reason is that the distance an electron travels between two scattering events (mean free path) is typically much larger than the atomic size. The electrons travel in an atomic sized conductor ballistically, and the resistance becomes independent of its length. In fact, the character of the resistance changes conceptually and it will be necessary to invoke the wave nature of the electrons in the conductor for a proper description. The chemical nature of the metallic elements starts to play an essential role as the size get smaller. As a consequence, while in the macroscopic world gold is a better conductor than lead by an order of magnitude, for conduction through a single atom, lead is better than gold by a factor of three. Metal nanowires display interesting quantum behavior, quantization of conductance, even at room temperature due to large energy level separation of the transport channels unlike in semiconductors. From a practical point of view, nanowires can be easily generated by putting in contact two metal surfaces,

which are subsequently pulled apart. During nanowire elongation and just before rupture, the conductance displays flat plateaus and abrupt jumps take a value of approximately one quantum conductance $G_0 = \frac{2e^2}{\hbar}$. The mechanical properties are also quite unusual: plastic deformation in a macroscopic metal occurs with dislocation motion. On the other hand, atomic size metal wires flow in response to applied stresses with structural rearrangements and their yield strength is one order of magnitude larger than bulk materials.

The invention and refinement of experimental techniques such as scanning tunnelling microscope (STM), high resolution transmission electron microscope (HRTEM) and mechanically controllable break junction (MCJB) have made the fabrication of such wires possible [1], [2]. The fabrication of the stable gold monatomic chains suspended between two electrodes is one of the milestones in nanoscience. Ohnishi *et al.* [1], visualized nanometric gold wires by the first time by transmission electron microscopy (TEM). Surprisingly, in a stable bridge of four atoms connecting two gold tips, the atoms spaced by 3.5-4 Å have been observed. These interatomic distances are much larger than interatomic distance in gold dimer (Au_2) and bulk Au. At the same time, gold monoatomic chain with a length of four or more atoms have produced by Yanson *et al.* [2], by using both STM and MCJB. They have used observed last conductance plateau during stretching (close to quantum conductance $\frac{2e^2}{\hbar}$) to decide that it has been a monoatomic chain. But they have not visualized the chains.

In this thesis, we have studied unusual mechanical and electronic properties of metal chain nanowires from first principles. In the first part, six different metals (Au, Ag, Al, Cu, Pt and Na) are studied in detail. All metals under study show two wire structures which are linear and zigzag structures. Au, Al and Pt show two different zigzag structures. All the wires are metallic. Relative stabilities are investigated by calculating the tension corresponding to applied force to keep the wire at a specific length. Au and Pt have bigger breaking force at breaking point relative to other metallic wires. In the second part, effects of H, H_2 and C impurities on mechanical and electronic properties of Au monoatomic chains are also studied. Except from Au-H system, i.e, when it contains C and H_2 impurities, wire becomes insulator. Before breaking, Au-impurity-Au bond

length is in the range of long interatomic distance observed in experiment. So, the presence of an impurity can explain the observed long interatomic distances. However, changing of bond lengths and breaking bond during the stretching of wire depends on the type of impurity. If one stretches the Au-H system, all bond lengths increase in the same amount before breaking. However in Au-C system, Au-Au bond length away from the C increases much more than other bonds. It is shown that absorption of impurity atoms modify the stiffness of the bonds in the wire. This is related to the charge transfer from Au to impurity (for H and C). In H and C systems, wire breaks from Au-Au bond away from the impurity. However in H_2 system, wire breaks from Au-H bond.

The thesis is organized as follows: Chapter 2 summarizes the theoretical background of the methods used in this thesis. In Chapter 3, some literature review is presented. In chapter 4 and 5 results are summarized. Finally, Chapter 6 concludes the thesis.

Chapter 2

THEORETICAL BACKGROUND

2.1 The problem of structure of matter

The microscopic description of the physical and chemical properties of matter is a complex problem. In general, we deal with a collection of interacting atoms, which may also be affected by some external field. This ensemble of particles may be in the gas phase (molecules and clusters), or in a condensed phase (solids, surfaces, wires), they could be solids, liquids or amorphous, homogeneous or heterogeneous (molecules in solution, interfaces, adsorbates on surfaces). However, in all cases we can certainly describe the system by a number of nuclei and electrons interacting through columbic (electrostatic) forces. Formally, we can write the Hamiltonian of such a system in the following general form:

$$H = \sum_{I=1}^{N} \frac{\overrightarrow{P_I^2}}{2M_I} + \sum_{i=1}^{N_e} \frac{\overrightarrow{p_i^2}}{2m} + \sum_{i>j} \frac{e^2}{|\overrightarrow{r_i} - \overrightarrow{r_j}|} + \sum_{I>J} \frac{Z_I Z_J e^2}{|\overrightarrow{R_I} - \overrightarrow{R_J}|} - \sum_{i,I} \frac{Z_I e^2}{|\overrightarrow{R_I} - \overrightarrow{r_i}|} \quad (2.1)$$

where $R = R_N$, $N = 1...N$, is a set of N nuclear coordinates, and $r = r_{N_e}$, $i = 1...N_e$, is a set of N_e electronic coordinates. Z_I and M_I are the N nuclear charges and masses, respectively. Electrons are fermions, so that the total electronic wave

function must be antisymmetric with respect to exchange of two electrons. Nuclei can be fermions, bosons or distinguishable particles, according to the particular problem under examination. All the ingredients are perfectly known and, in principle, all the properties can be derived by solving the many-body Schrödinger equation:

$$\widehat{H}\Phi(x, \overrightarrow{R}) = E\Phi(x, \overrightarrow{R}) \tag{2.2}$$

where $x \equiv (\overrightarrow{r}, s)$ full set of electronic positions and spin variables. In practice, this problem is almost impossible to treat in a full quantum mechanical framework. Only in a few cases a complete analytic solution is available, and numerical solutions are also limited to a very small number of particles. There are several features that contribute to this difficulty. First, this is a multicomponent many-body system, where each component (each nuclear species and the electrons) obeys a particular statistics. Second, the complete wave function cannot be easily factorized because of coulombic correlations. In other words, the full Schrödinger equation cannot be easily decoupled into a set of independent equations so that, in general, we have to deal with $(3N + 3N_e)$ coupled degrees of freedom. The dynamics is an even more difficult problem, and very few and limited numerical techniques have been proposed to solve it. The usual choice is to find out some proper approximations. The majority of the calculations presented in the literature are based on: (1) the adiabatic separation of nuclear and electronic degrees of freedom (adiabatic approximation), and (2) the classical treatment of the nuclei.

2.2 Adiabatic approximation (Born-Oppenheimer approximation)

The first observation is that the time scale associated with the motion of the nuclei is usually much slower than that associated with electrons. In fact, the small mass of the electrons as compared to that of the protons is about 1 in 1836, meaning that their velocity is much larger. In this case, it was proposed in the early times of quantum mechanics that the electrons can be adequately described

as following instantaneously the motion of the nuclei, staying always in the same stationary state of the electronic Hamiltonian. This stationary state will vary in time because of the coulombic coupling of the two sets of degrees of freedom but, if the electrons were, e.g. in the ground state, they will remain there forever. This means that as the nuclei follow their dynamics, the electrons instantaneously adjust their wave function according to the nuclear wave function. Under the above conditions, the full wave function factorizes in the following way:

$$\Phi(x, \overrightarrow{R}) = \Psi(x, \overrightarrow{R})\chi(\overrightarrow{R}) \tag{2.3}$$

where $\Psi(x, \overrightarrow{R})$ is the electronic wave function, $\chi(\overrightarrow{R})$ is the nuclear wave function. $\Psi(x, \overrightarrow{R})$ is more localized than $\chi(\overrightarrow{R})$. That is $\nabla_I \chi(\overrightarrow{R}) \gg \nabla_I \Psi(x, \overrightarrow{R})$. $\Psi(x, \overrightarrow{R})$ is normalized for every R. So this separation of variables leads to

$$[T_e + V_{ee}(\overrightarrow{r}) + V_{eN}(\overrightarrow{r}, \overrightarrow{R})]\Psi_n(x, \overrightarrow{R}) = \varepsilon_n(\overrightarrow{R})\Psi_n(x, \overrightarrow{R}) \tag{2.4}$$

and

$$[T_N + V_{NN}(\overrightarrow{R}) + \varepsilon(\overrightarrow{R})]\chi(\overrightarrow{R}) = E(\overrightarrow{R})\chi(\overrightarrow{R}) \tag{2.5}$$

Electronic eigenvalue $\varepsilon_n(\overrightarrow{R})$ depends parametrically on the ionic positions $\overrightarrow{R}$. In Adiabatic approximation, ions move on the potential-energy surface of the electronic ground state only.

$$[T_e + V_{ee}(\overrightarrow{r}) + V_{eN}(\overrightarrow{r}, \overrightarrow{R})]\Psi_0(x, \overrightarrow{R}) = \varepsilon_0(\overrightarrow{R})\Psi(x, \overrightarrow{R}) \tag{2.6}$$

and

$$[T_N + V_{NN}(\overrightarrow{R}) + \varepsilon(\overrightarrow{R})]\chi(\overrightarrow{R}) = i\hbar\frac{\partial}{\partial t}\chi(\overrightarrow{R}, t) \tag{2.7}$$

2.3 Classical nuclei approximation

Solving any of the two last equations 2.6 or 2.7 is a difficult task for two reasons: First, it is a many-body equation in the $3N$ nuclear coordinates, the

interaction potential being given in an implicit form. Second, the determination of the potential energy surface $\varepsilon_n(\overrightarrow{R})$ for every possible nuclear configuration R involves solving L^{3N} times the electronic equation, where L is a typical number of grid points. The largest size achieved up to date using non-stochastic methods is six nuclear degrees of freedom. In a large variety of cases of interest, however, the solution of the quantum nuclear equation is not necessary. This is based on two observations: (1) The thermal wavelength for a particle of mass M is $T = \frac{e^2}{Mk_BT}$ so that regions of space separated by more than $\lambda_T \simeq 0.1$ Å do not exhibit quantum phase coherence. The least favorable case is that of hydrogen, and even so, at room temperature $\lambda_T \simeq 0.1$ Å , while inter-atomic distances are normally of the order of 1 Å. (2) Potential energy surfaces in typical bonding environment are normally stiff enough to localize the nuclear wave functions to a large extent. For instance, a proton in a hydroxyl group has a width of about 0.25 Å. This does not mean that quantum nuclear effects can be neglected altogether. In fact, there is a variety of questions in condensed matter and molecular physics which require a quantum mechanical treatment of the nuclei. Well-known examples are the solid phases of hydrogen, hydrogen-bonded systems like water and ice, fluxional molecules, and even active sites of enzymes. There is, however, an enormous number of systems where the nuclear wave packets are sufficiently localized to be replaced by Dirac's δ-functions. The connection between quantum and classical mechanics is achieved through Ehrenfest's theorem for the mean values of the position and momentum operators. The quantum-mechanical analog of Newton's equations is:

$$\frac{< \partial^2 \overrightarrow{P_I} >}{\partial t^2} = - < \nabla_I E_0(\overrightarrow{R}) > \tag{2.8}$$

and

$$E_0(\overrightarrow{R}) = \varepsilon_0(\overrightarrow{R}) + V_{NN}(\overrightarrow{R}) \tag{2.9}$$

Force $-\nabla_I E_0(\overrightarrow{R})$ contains contributions from direct ion-ion interaction and from the gradient of the electronic total energy.

2.4 Hartree and Hartree-Fock approximation

Solving the Schrödinger equation of a system of N_e interaction electrons in the external coulombic field created by a collection of atomic nuclei is a very difficult task. The exact solution is known only in the case of uniformly electron gas, for atoms with a small number of electrons, and for a few small molecules. These exact solutions are always numerical. At the analytic level, approximations must be used. The first approximation may be considered the one proposed by Hartree. It consists of postulating that the many-electron wave function can be written as a simple product of one-electron wave functions [3]. Each of these verifies a one-particle Schrödinger equation in an effective potential that takes into account the interaction with the other electrons in a mean field way:

$$\Psi(x, \overrightarrow{R}) = \prod_i \phi_i(\overrightarrow{r_i}) \tag{2.10}$$

and

$$(-\frac{\hbar^2}{2m}\nabla^2 - \frac{Ze^2}{r} + \int \frac{\sum_{j\neq i} |\phi_j(\overrightarrow{r'})|^2}{|\overrightarrow{r} - \overrightarrow{r'}|} d^3r')\phi_i(\overrightarrow{r}) = \varepsilon_i \phi_i(\overrightarrow{r}) \tag{2.11}$$

where third term in left hand side is the Hartree potential. Sum of the second and the third term is the effective potential. Notice that charge density $n_j = |\phi_j|^2$ does not include the charge associated with particle i, so that the Hartree approximation is (correctly) self-interaction free. In this approximation, the energy of the many-body system is not just the sum of the eigenvalues of equations(2.11) because the formulation in terms of an effective potential makes the electron-electron interaction counted twice. The correct expression for the energy is:

$$E^H = \sum_i^{N_e} \varepsilon_i - \frac{1}{2}\int\int \frac{n(\overrightarrow{r})n(\overrightarrow{r'})}{|\overrightarrow{r} - \overrightarrow{r'}|} d^3r d^3r' = \frac{<\Psi|H|\Psi>}{<\Psi|\Psi>} \tag{2.12}$$

The set of N_e coupled partial differential equations (2.11) can be solved by minimizing the energy with respect to a set of variational parameters in a trial wave function

$$\delta \frac{<\widetilde{\Psi}|H|\widetilde{\Psi}>}{<\widetilde{\Psi}|\widetilde{\Psi}>} = 0$$

or, alternatively, by recalculating the electronic densities using the solutions of eqn. 2.11, then calculating the potential, and solving again the Schrödinger equation. This procedure can be repeated several times, until self-consistency in the initial and final wave function or potential is achieved. This procedure is called self-consistent field (SCF) method. The Hartree approximation treats the electrons as distinguishable particles. However, the wave function of a many electron system must be antisymmetric under exchange of two electron because the electrons are fermions. The antisymmetry of the wave function produces a spatial separation between electrons that have the the same spin and thus reduces the Coulomb energy of the electronic system. Slater determinant is the way to make antisymmetrized many electron wave function by using Pauli exclusion principle (Fermi statistics for electrons):

$$\Psi_{i_1...i_{N_e}}(q_1...q_{N_e}) = \frac{1}{\sqrt{N_e}} \begin{pmatrix} \phi_{i_1}(q_1) & \dots & \phi_{i_{N_e}}(q_{N_e}) \\ \vdots & & \vdots \\ \phi_{i_1}(q_1) & \dots & \phi_{i_{N_e}}(q_{N_e}) \end{pmatrix} \tag{2.13}$$

$$= \frac{1}{\sqrt{N_e}} \sum_P (-1)^P P\phi_{i_1}(q_1)...\phi_{i_{N_e}}(q_{N_e}) \tag{2.14}$$

This wave function allows particle exchange due to the antisymmetry of wave function. The energy of the system is reduced by this exchange of particles (electrons). The approximation is called Hartree-Fock approximation (HF) [3], and has been the way of choice of chemists for calculating the electronic structure of molecules for a long time. In fact, it provides a very reasonable picture for atomic systems and, although many-body correlations (arising from the fact that, due to the two-body Coulomb interactions, the total wave function cannot necessarily be separated as a sum of products of single-particle wave functions) are completely absent, it also provides a reasonably good description of inter-atomic bonding. Hartree-Fock equations look the same as Hartree equations, except for the fact that the exchange integrals introduce additional coupling terms in the below equations:

$$(-\frac{\hbar^2}{2m}\nabla^2 - \frac{Ze^2}{r} + e^2 \sum_{i \neq j} \int \frac{|\phi_j(\overrightarrow{r'})|^2}{|\overrightarrow{r} - \overrightarrow{r'}|} d^3r')\phi_i(\overrightarrow{r})$$

$$- \quad e^2 \sum_{j \neq i} \int \frac{\phi_j^\star(\overrightarrow{r'})\phi_i(\overrightarrow{r})}{|\overrightarrow{r} - \overrightarrow{r'}|} d^3r' \phi_j(\overrightarrow{r})) = \varepsilon_i \phi_i(\overrightarrow{r}) \quad (2.15)$$

Notice that also in Hartree-Fock the self-interaction cancels exactly.

2.5 Thomas-Fermi theory

Thomas and Fermi proposed [3], at about the same time as Hartree (1927-1928), that the full electronic density was the fundamental variable of the many-body problem, and derived a differential equation for the density without using to one-electron orbitals. The Thomas-Fermi approximation was actually too incomplete because it did not include exchange and correlation effects, and was also unable to sustain bound states because of the approximation used for the kinetic energy of the electrons. However, it set up the basis for the later development of Density Functional Theory (DFT), which has been the way of choice in electronic structure calculations in condensed matter physics during the past twenty years.

Thomas and Fermi (1927) gave a way for constructing the total energy in terms only of the electronic density. They used the expression for the kinetic, exchange and correlation energies of the homogeneous electron gas to construct the same quantities for the inhomogeneous system in the following way $E_i = \int \varepsilon_i[n(\overrightarrow{r})]dr$ where $\varepsilon_i \sim \varepsilon[n(\overrightarrow{r})]$ is the energy density (corresponding to the piece i), calculated locally for the value of the density at that point in space. This was the first time that the local density approximation, or LDA, was used. For the homogeneous electron gas the density is related to the Fermi energy (ε_F) by

$$n = \frac{1}{3\pi^2}(\frac{2m}{\hbar^2})^{3/2}\varepsilon_F^{3/2} \quad (2.16)$$

The kinetic energy density of the homogeneous gas is

$$T = \frac{3n\varepsilon_F}{5}$$

so that the kinetic energy density is:

$$t[n] = \frac{3}{5}\frac{\hbar^2}{2m}(3\pi^2)^{3/2}n^{3/2} \quad (2.17)$$

The kinetic energy is written,

$$T^{TF} = C_K \int n^{5/3}(\overrightarrow{r})d^3r \tag{2.18}$$

with $C_K = 3(3\pi^2)^{2/3}/10$. The inhomogeneous system is thought of as locally homogenous. Neglecting exchange and correlation in total energy expression we obtain Thomas - Fermi theory:

$$E_{TF}[n] = C_K \int n^{(5/3)}dr + \int v(r)n(\overrightarrow{r})dr + \frac{1}{2}\int\int \frac{n(\overrightarrow{r})n(r')}{|\overrightarrow{r} - \overrightarrow{r'}|}d^3rd^3r' \tag{2.19}$$

It can be seen that E_{TF} depends only on the electronic density, it is a functional of the density. By using variational principle, one can obtain the density $n(r)$ which minimizes E_{TF} subjected to the constraint that the total integrated charge be equal to the number of electrons. This can be put in terms of functional derivatives:

$$\frac{\delta}{\delta n(\overrightarrow{r})}[E_{TF} - \mu \int n(\overrightarrow{r})d^3r] = 0 \tag{2.20}$$

with

$$\mu = \frac{5}{3}C_K n^{2/3}(\overrightarrow{r}) + v(\overrightarrow{r}) + \int \frac{n(\overrightarrow{r}')}{|\overrightarrow{r} - \overrightarrow{r'}|}d^3r \tag{2.21}$$

where μ is the chemical potential.

Hartree equation describes the ground states better than Thomas-Fermi theory. The differences between them lay in the different treatments of the kinetic energy T.

2.6 Density Functional Theory

The density functional theory (DFT), developed by Hohenberg and Kohn [4], and Kohn and Sham [5], has provided a way to treat the problem of describing the effects of exchange and correlation in an electronic system. The Coulomb energy of the electronic system can be reduced below its Hartree-Fock value if electrons that have the opposite spins and are also spatially separated. In this case the Coulomb energy of the electronic system is reduced at the cost of increasing the kinetic energy of the electrons. The differences between the many body energy of

an electronic system and the energy of the system calculated in the Hartre-Fock approximation is called the correlation energy. Hohenberg and Kohn proved that the total energy, including exchange and this correlation energy, of an electron gas even under the influence of an external static potential, for our case the potential due to ions, is a unique functional of the electron density. Further, the minimum value of the total energy functional is the ground-state energy of the system, and the density that yields this minimum value is the exact ground state energy. In addition to this, Kohn and Sham showed how to replace the many-electron problem by an exactly equivalent set of self-consistent single electron equations. Self-consistent here means that the solutions determine the equations themselves.

The important distinction between Hartree-Fock approximation and the Hohenberg-Kohn theory is the initial approach to the problem. Hartree-Fock method initially approximates a set of single-electron wave functions, anti- symmetrized by the Slater determinant approach and minimizes the total energy in terms of these functions. However, in the density functional theory, the total energy is introduced as a functional of the charge density, which is introduced ad-hoc to the system. The charge density later is definable as the sum of single-electron densities, whence the derivation of total energy with respect to the charge density yields the Kohn-Sham equations.

2.6.1 The Hohenberg-Kohn Theory

In 1964, P. Hohenberg and W. Kohn [4] formulated and proved a theorem on the ground of Thomas-Fermi theory. The theorem divided into two parts:

1. The ground-state energy of a many body system is a unique functional of the particle density, $E_0 = E[(\overrightarrow{r})]$. There is no $v(r) \neq v'(\overrightarrow{r})$(external potential) that corresponding to the same electronic density for the ground state.

2. The functional $E[(\overrightarrow{r})]$ has its minimum relative to variations $\delta n(r)$ of the particle density at equilibrium density $n_0(\overrightarrow{r})$.

$$E = E[n_0(\overrightarrow{r})] = minE[(\overrightarrow{r})] \tag{2.22}$$

2.6.2 The Hohenberg-Kohn variational principle

The most important property of an electronic ground state is its energy. By wave function methods E could be calculated by direct approximate solution of the Schrödinger equation or the Rayleigh-Ritz minimal principle,

$$E = min_{\widetilde{\Psi}}(\widetilde{\Psi}, H\widetilde{\Psi}) \tag{2.23}$$

where $\widetilde{\Psi}$ is a normalized trial wave function for the given number of electrons N_e.

The formulation of minimal principle in terms of trial densities $n(r)$, rather than trial wave function $\widetilde{\Psi}$ was first presented by Hohenberg-Kohn [4].

Every trial function $\widetilde{\Psi}$ corresponding to a trial density $n(r)$ obtained by integrating $\widetilde{\Psi}\widetilde{\Psi^{\star}}$ over all variables expect the first and multiplying by N_e. One may carry out the minimization in two stages. First fix trial density and denote $\widetilde{\Psi_n^i}$ a the class of trial functions with n. We define the constrained energy minimum, with n fixed, as

$$E_v[\widetilde{n}(\overrightarrow{r})] \equiv min_i(\widetilde{\Psi_{\widetilde{n}}^i}, H\widetilde{\Psi_{\widetilde{n}}^i}) = \int v(\overrightarrow{r})\widetilde{n}(\overrightarrow{r})dr + F[n(\overrightarrow{r})] \tag{2.24}$$

where

$$F[\widetilde{n}(\overrightarrow{r})] = min_i[\widetilde{\Psi_{\widetilde{n}}^i}, (T+U)\widetilde{\Psi_{\widetilde{n}}^i}] \tag{2.25}$$

$F[n(\overrightarrow{r})]$ requires no explicit knowledge of $v(r)$. It is a universal functional of the density $\widetilde{n}(r)$.

2.6.3 The self-consistent Kohn-Sham equations

$$E_{v(\overrightarrow{r})}(\widetilde{n}(\overrightarrow{r})) \equiv \int v(\overrightarrow{r})\widetilde{n}(\overrightarrow{r})dr + T[\widetilde{n}(\overrightarrow{r})] \tag{2.26}$$

The Euler-Lagrange equations, embodying the fact the expression $n(\overrightarrow{r}) = \sum_i^{N_e} |\varphi_i(\overrightarrow{r})|^2$ is stationary with respect to variations of $\widetilde{n}(\overrightarrow{r})$ which leave the total number of electrons unchanged, is

$$\delta E_{v(\overrightarrow{r})}[\widetilde{n}(\overrightarrow{r})] = \int \delta\widetilde{n}(\overrightarrow{r})\{v(\overrightarrow{r}) + \frac{\delta}{\delta\widetilde{n}(\overrightarrow{r})}T[\widetilde{n}(\overrightarrow{r})]|_{\widetilde{n}\equiv n} - \varepsilon\}dr \tag{2.27}$$

where $\widetilde{n}(\overrightarrow{r})$ is the exact ground-state density for $v(r)$. Here ε is a Lagrange multiplayer to assure particle conservation. Now in this soluble, noninteracting case, the ground state energy and density can be obtained by calculating the eigenfunctions φ_i and eigenvalues ε_i of noninteracting single-particle equations

$$(-\frac{\hbar^2}{2m}\nabla^2 + v(\overrightarrow{r}) - \varepsilon_i)\varphi_i = 0 \tag{2.28}$$

yielding

$$E = \sum_{i=1}^{N_e} \varepsilon_i \tag{2.29}$$

and

$$n(\overrightarrow{r}) = \sum_{i}^{N_e} |\varphi_i(\overrightarrow{r})|^2 \tag{2.30}$$

Here i labels both orbital quantum numbers and spin.

The Kohn-Sham total energy functional for a set of doubly occupied electronic state φ_i can be written

$$E[n(\overrightarrow{r})] = \int v(\overrightarrow{r})n(\overrightarrow{r})d^3r + F[n(r)] \tag{2.31}$$

where functional $F[\widetilde{n}(\overrightarrow{r})]$ is written in the form of

$$F[\widetilde{n}(\overrightarrow{r})] = T[\widetilde{n}(\overrightarrow{r})] + \frac{1}{2}\int\int \frac{\widetilde{n}(\overrightarrow{r})\widetilde{n}(\overrightarrow{r}')}{|\overrightarrow{r} - \overrightarrow{r}'|}d^3r d^3r' + E_{XC}[\widetilde{n}(\overrightarrow{r})] \tag{2.32}$$

$T[\widetilde{n}(\overrightarrow{r})]$ is the kinetic energy functional for noninteracting electrons and is in form of

$$T[n(r)] = 2\sum_i \int \varphi_i[-\frac{\hbar^2}{2m}]\nabla^2\varphi_i d^3r \tag{2.33}$$

The last term is the exchange-correlation energy functional. The corresponding Euler-Lagrange equation, for a given total number of electrons, has the form

$$\delta E_{v(\overrightarrow{r})}[\widetilde{n}(\overrightarrow{r})] = \int \delta\widetilde{n}(\overrightarrow{r})\{v_{eff}(\overrightarrow{r}) + \frac{\delta}{\delta\widehat{n}(\overrightarrow{r})}T[\widetilde{n}(\overrightarrow{r})]|_{\widetilde{n}(\overrightarrow{r})=n(\overrightarrow{r})} - \varepsilon\}d^3r = 0 \tag{2.34}$$

with

$$v_{eff}(\overrightarrow{r}) = v(\overrightarrow{r}) + \int \frac{n(\overrightarrow{r}')}{|\overrightarrow{r} - \overrightarrow{r}'|}d^3r' + v_{XC}(\overrightarrow{r}) \tag{2.35}$$

and

$$v_{XC} \equiv \frac{\delta}{\delta\widetilde{n}(\overrightarrow{r})}E_{XC}[\widetilde{n}(\overrightarrow{r})]|_{\widetilde{n}(\overrightarrow{r})=n(\overrightarrow{r})} \tag{2.36}$$

The form of eqn. 2.31 is identical to eqn. 2.26 for noninteracting particles moving in an effective external potential v_{eff} instead of $v(\overrightarrow{r})$ and the minimizing density $n(\overrightarrow{r})$ is given by solving the single particle equation

$$(-\frac{\hbar^2}{2m}\nabla^2 + v_{eff} - \varepsilon_i)\varphi_i = 0 \tag{2.37}$$

These self-consistent equations are called the Kohn-Sham (KS) equations and the ground state energy is given by

$$E = \sum_i \varepsilon_i + E_{XC}[n(\overrightarrow{r})] - \int v_{XC} n(\overrightarrow{r}) d^3r - \frac{1}{2}\int \frac{n(\overrightarrow{r})n(\overrightarrow{r'}))}{|\overrightarrow{r}\,\overrightarrow{r'}|} d^3r d^3r, \tag{2.38}$$

If E_{XC} and v_{XC} is neglected, the Kohn-sham equations reduce to self consistent Hartree equations. With the exact E_{XC} and v_{XC} all many body effects are in principle included. The Kohn-Sham equations must be solved self consistently so that the occupied electronic states generate a charge density that produces the electronic potential that was used to construct the equations.

2.7 Pseudopotential Approximation

Mathematically and numerically, a plane-wave-basis formalism is one of the simplest and most natural formalism to implement for crystals. However, expanding the core wave functions or the core oscillatory region of the valence wave functions with plane waves is extremely inefficient. Therefore, plane-wave basis sets are practically always used in conjunction with the pseudopotential approximation. The combination of pseudopotentials and plane waves has become one of the most popular methods for electronic structure calculations. The physical reasoning behind the pseudopotential approximation is simple: since the core-electron wave functions of an atom remain essentially unchanged when placed into different chemical environments and since the only major contribution of core wave functions to chemical bonding is to enforce the orthogonality of the valence wave functions to the core states, the true atomic potential can be replaced by a pseudopotential that effectively reproduces the effects of the core electrons. But with only this physical constraint, i.e removing the core electrons but reproducing exactly all electron properties after a certain cutoff radius, an infinite number of

pseudopotentials can be generated.

It is well known that the most physical properties of solids are dependent on the valence electrons to a much greater than core electrons. The pseudopotential approximation exploits this by removing the core electrons, which are highly localized, and by replacing them and the strong ionic potential by a weaker pseudopotential that acts on a set of pseudofunctions rather than the true valence wave functions. The valence wave function oscillate rapidly in the region occupied by the core electrons due to the strong ionic potential in this region. These oscillations maintain the orthogonality between the core wave functions and the valence wave functions due to exclusion principle. Since the kinetic energy of a state is proportional to second derivative of the wave function the kinetic energy

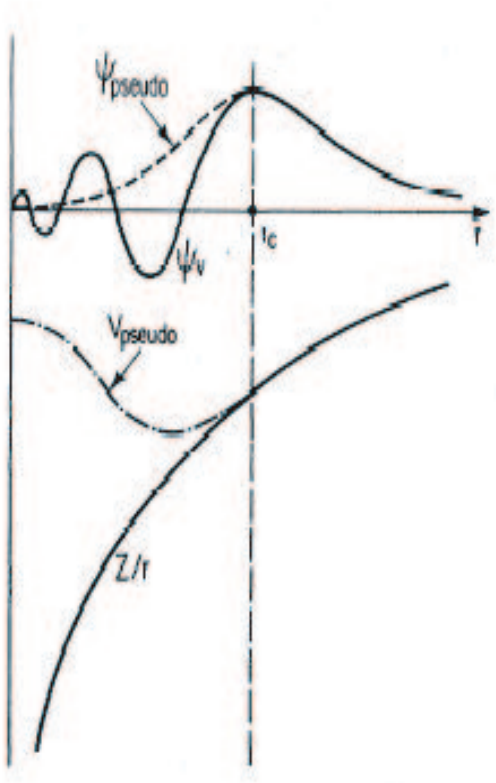

Figure 2.1: Schematic illustration of all-electron (solid lines) and pseudoelectron (dashed lines) potentials and their corresponding wave functions. The radius at which all-electron and pseudopotential values match is designated r_c.

of the free electron state is increased in the vicinity of the core region. Most pseudopotentials are then constructed such that they satisfy four general conditions. The first is that the valence pseudowavefunctions generated from the pseudopotential should contain no nodes. This stems from the fact that we would like to construct smooth pseudowavefunctions. Second, the normalized atomic radial pseudo-wave-function (PP) with angular momentum l is equal to the normalized radial all-electron wave function (AE) beyond a chosen cutoff radius r_{cl}

$$R_l^{cl}(r) = R_l^{AE}(r) \; for \; r_{cl} > r \tag{2.39}$$

Third, the charge enclosed within r_{cl} for the two wave functions must be equal

$$\int_0^{r_{cl}} |R_l^{PP}(r)|^2 r^2 dr = \int_0^{r_{cl}} |R_l^{AE}(r)|^2 r^2 dr \tag{2.40}$$

Last, almost redundantly, the valence all-electron and pseudopotential eigenvalues must be equal,

$$\varepsilon_l^{PP} = \varepsilon_l^{AE} \tag{2.41}$$

If a pseudopotential meets the conditions outlined above, it is commonly referred to as a norm-conserving pseudopotential. Pseudopotential is angular momentum dependent so each angular momentum component of the wave function see a different potential. So its scattering properties for the pseudo wave function are identical to scattering properties of the ion and the core electrons for the valence wave functions.

Chapter 3

REVIEW OF THE FIELD

3.1 Experimental Results for gold nanowires

By high resolution transmission electron microscopy (HR-TEM), it is possible to resolve individual atoms for the heavier elements. Ohnishi, Kondo and Takayanagi [1] used this capability by combining their ultra-high vacuum HR-TEM setup with two different manipulation techniques to produce atomic wires. First, they constructed a miniature STM that fits into the specimen space of the TEM. It is fascinating to see the atomically-resolved video images they show that a tip scanning a sample surface, and subsequently indenting it. When retracting a gold tip from a gold sample the group observed that the connecting bridge gradually thins down, as seen figure 3.1.

All experiments are performed at room temperature, giving the atoms enough mobility to optimize the configuration, and as a result it is seen that the bridge connecting the two electrodes, oriented along the [110] direction, often consists of a straight wire section. As the number of atomic rows in the connecting nanowire decreases the conductance is also seen to decrease in a step-wise fashion, as expected. The conductance of a one atom strand in the images is close to $\frac{2e^2}{\hbar}$. Evidence for this interpretation is obtained by analyzing the contrast profile in the images.

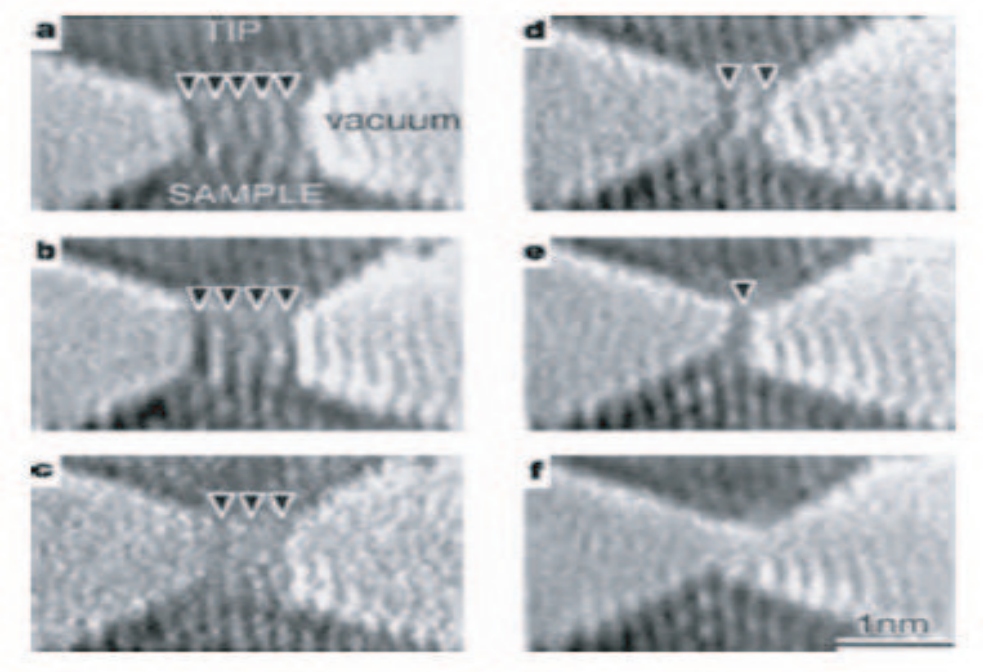

Figure 3.1: TEM images of a gold contact recorded while withdrawing the tip from the surface. A gold bridge formed between the gold tip (top) and the sample (bottom) thins down when going from (a) to (e), where conductance drops to $2G_0$. The contact finally break at (f), for which conductance drop to zero. Taken from [1].

In order to resolve the individual atoms in the chain a second technique was employed. In this technique, the STM was replaced by a very thin gold film specimen, where an intense electron beam current was used to melt two adjacent holes in this film. For [110] oriented films a gold bridge along the [001] direction between these two holes was seen to evolve into an atomic chain that survived for about two minutes, see figure 3.2.

Note that in this configuration the conductance of the chain cannot be measured. Remarkably, the spacing between the atoms in the chain was found to be $0.35 - 0.4$ nm, much larger than the nearest neighbor distance in bulk gold, 0.288 nm. This value is much larger than any theoretical calculation predicts, since the overlap between the electron clouds of the gold atoms is too small to provide sufficient stability for the atomic chain.

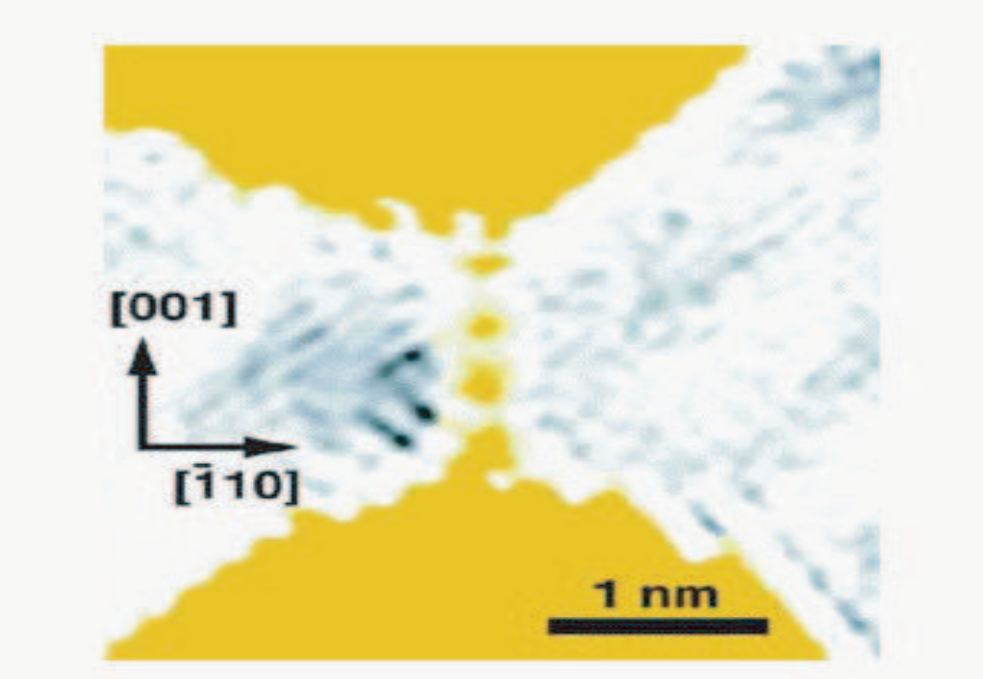

Figure 3.2: TEM images of a gold atomic chain forming between two gold banks. Taken from [1].

The second paper in the 1998 issue of Nature [2] used different techniques in several important aspects. The atomic structure was not imaged directly, but the formation of chains was deduced from the experimental observations of the conductance as a function of stretching. The advantages, on the other hand, are the low temperature (4.2 K) at which the experiment is performed. This allows for a long-term stability of the gold atomic chains so that detailed spectroscopy can be done. In addition, the cryogenic vacuum conditions avoid any contamination on the nanowires.

By standard low-temperature STM and MCBJ techniques atomic-sized contacts of gold were produced. In contrast to many other metals, for Au it was found that the last conductance plateau, at a value of ~ 1 G_0, can often be stretched far beyond a length corresponding to an atomic diameter. An example is presented in figure 3.3, where a plateau of about 2 nm length is found. Since it has been established that the conductance is predominantly determined by the

narrowest cross section, and that a single-atom contact for Au has a conductance near 1 G_0, due to this observation Yanson *et al.* [2], speculate that a chain of atoms was being formed. This is indeed very surprising, even more so than in the case of the room temperature TEM experiments. For the latter, at an earlier stage the atoms have enough mobility to produce a stable, straight nanowire several atoms in cross section, and the atomic rows in the wire are removed one after the other by thermal diffusion of the atoms on the surface. This leaves a single atomic row standing before contact is finally lost. However, at low temperatures the atomic structure is frozen into the configuration in which it lands after an atomic rearrangement, forced by the stretching of the contact. When arriving at a single atom contact one would expect the contact to break at this weakest spot. Instead, atoms are apparently being pulled out of the banks to join in the formation of a linear atomic arrangement. Clearly, it is important to critically evaluate the interpretation of atomic chain formation.

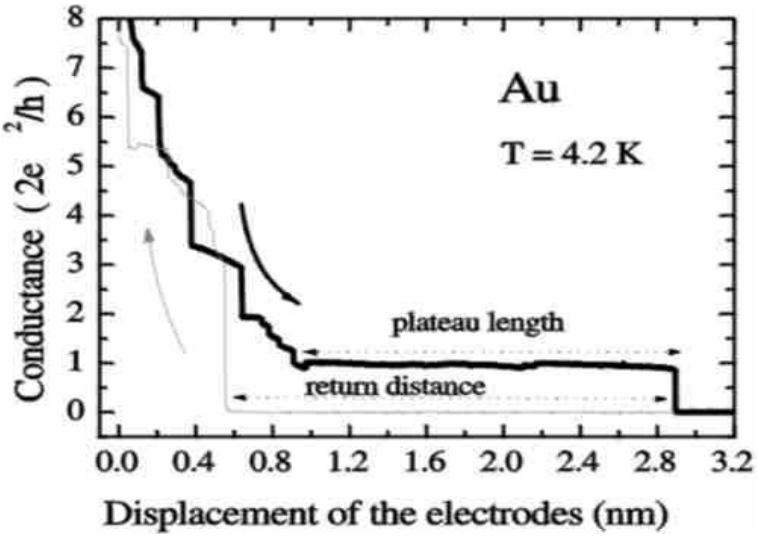

Figure 3.3: The conductance as a function of the displacement of the two gold electrodes with respect to each other in an MCBJ experiment at 4.2 K. The trace starts at the upper left, coming from higher conductance values (thick) curve. A long plateou with a conductance near 1 G_0 is observed and after jump to tunnelling one needs to return by a little more than the length of the long plateau to come back into contact(thin curve) [2].

A simple test involves recording the distance required to bring the electrodes

back into contact after the conductance has suddenly dropped to zero, as at the end of the plateau in figure 3.3. We imagine that a chain has formed, which finally ruptures at this moment. The atoms in the chain are then expected to fall back onto the banks, which implies that the separation between the electrodes should be approximately equal to the length of the chain, being approximately the length of the plateau. Figure 3.3 illustrates that this is indeed the case for this particular example, although one may anticipate variations in the return length according to the actual arrangement of the atoms after the collapse. By recording many curves similar to the one in figure 3.3, Yanson *et al* [2], obtained an average return distance as a function of the length of the last plateau. They observed a linear dependence of the return distance on the plateau length, with a slope between 1.0 and 1.3 and an offset of about 0.5 nm. The latter can be understood in terms of the elastic deformation of the banks: Even when no chain is formed and the contact breaks at a single atom, the atomic structure relaxes after rupture of the contact, giving rise to a finite return length.

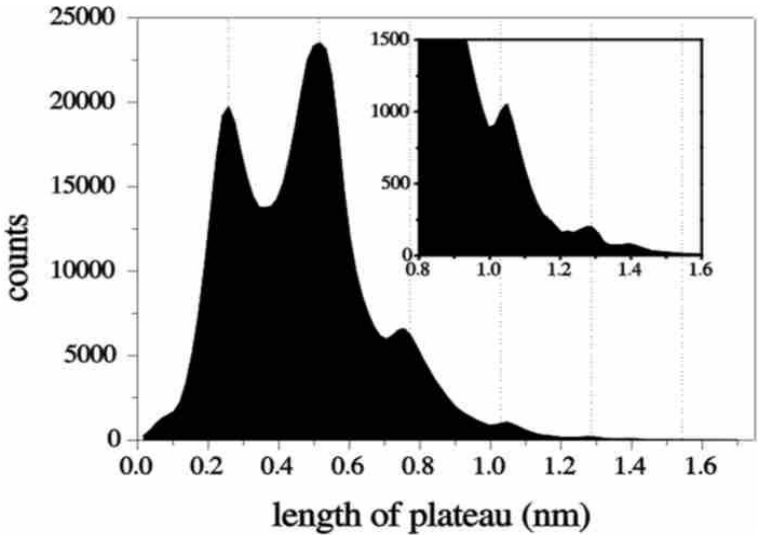

Figure 3.4: Distribution of plateau lengths for monoatomic chain [2].

Further evidence for the chain structure comes from an analysis of the distribution of lengths of the last conductance plateaus for many cycles of contact breaking. Figure 3.4 shows a histogram of plateau lengths. It is seen that the probability for early breaking is very low, it then rises to a first peak at 2.5 Å

length, after which it drops before rising to a second peak, which is usually higher than the first.

After the second peak the distribution of lengths drops steeply, but shows three additional peaks in the tail. The peak distance of $0.25-0.26$ nm agrees with the expected bond distance in a chain of gold atoms and the natural interpretation of the peaks in the length histogram is in terms of a preferential breaking of the chain at lengths corresponding to an integer number of atoms in the chain. The peaks in the distribution are broadened by the variation in starting and end configurations of the banks connecting the chain. In fact, a strict periodicity of the peaks would not be expected to continue much further than the first few, because the atoms making up the chain are removed from the banks, which then become, shorter. Occasionally plateaus of up to 2 nm in length have been found, which suggests that the system can self assemble chains of up to $7-8$ atoms long. It is often possible to obtain similar peak structure in a histogram of return distances.

Several explanations have been proposed in order to explain large interatomic distances observed in experiments. One proposal is based on the observation that the calculated equilibrium structure for a Au monatomic chain appears to have a zigzag geometry. Sanchez-Portal *et al.* [6, 7], proposed that every second atom in the zigzag chain could be thermally excited into a spinning motion around the chain axis, which would blur their image and TEM missed this image. On the other hand, Koizumi *et al.* [8], show that spinning atom around the chain axis may be seen by comparing the experimental images to simulations. They did not find strong evidence for spinning gold atoms. Other explanations involve the presence of 'impurity atoms', such as C, O, S, or H [9, 10, 11, 12, 13]. The simulations [8] suggest that adatoms of Si and S would be resolved, but the contrast for C (and O) would not exceed the noise level. It is known that regular gold surface is not very reactive, while the low-coordination gold atoms in the chain bind strongly to different species, as shown by first-principles calculations [9], [10]. Despite the high vacuum conditions of the experiment, there might be small amounts of adsorbed molecules running over the surface, and these will stick preferentially at the strong binding sites in the gold chain. Oxygen would be a good candidate,

since it would not be resolved in the images and the calculations suggest that a Au-O-Au-O chain would have Au-Au distance close to the observed values and the chain would be conducting, with a single open channel [10].

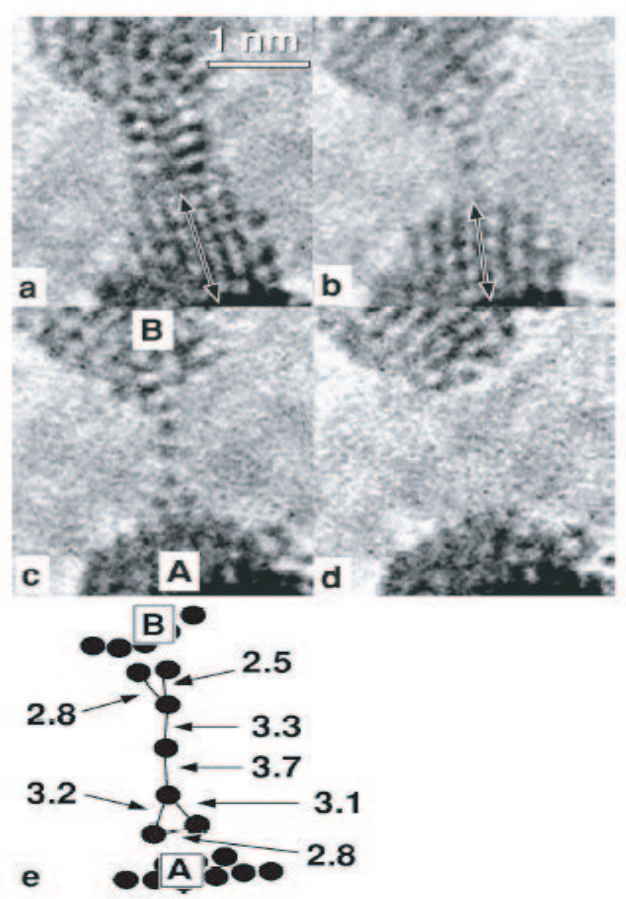

Figure 3.5: Time sequence of atomic resolution images of the formation, elongation and fracture of a suspended chain of gold atoms. Atomic positions appear as dark lines or dots. A schematic representation of the chain is shown in (e); the letters A and B indicate the apex position in (c). The double arrows in (a) and (b) have indicated that the movement of the lower apex. Taken from [14].

The experimental observation of the atomic chain formation and the long interatomic distances have been confirmed in an independent experiment by Rodrigues and Ugarte [14], using the thin-film double-hole technique. Similarly, their results [14] did not support rotating zigzag model of Sanchez-Portal [6]. They have claimed that the rotation of a high atomic number atom, such as

gold, would generate ghost dots, which would easily be detected. The large and irregular bond lengths observed suggest the presence of light interstitial atoms that may stabilize the chains [11]. In high resolution images taken with a new generation defocus-imaging modulation processing electron microscope by Takai *et al.* [15], much smaller Au-Au distances of $0.25 - 0.29$ nm were found.

A further study by Kizuka *et al.* [16], appears to be at variance with most of the earlier results. Here, a miniature STM is operated inside a HR- TEM at regular vacuum conditions. Again, for gold it is frequently observed that upon separation of the contact between tip and sample it ends with the formation of a chain of atoms. Similar to the results of Takai *et al.* [15], a distance of only 0.27 ± 0.02 nm was obtained between the atoms in the chain, which can be stretched to the break point (0.3 ± 0.02 nm). Surprisingly, the atomic wires were found to be insulating. At the moment when the structure is seen to jump from a multiatom cross section to a single atom chain the conductance drops to zero. Moreover, the chains were found to be bent even under stretched conditions. Very long atomic chains, up to 10 atoms in a row, were observed. They were stable for longer times than reported before. Although the authors make a few suggestions to explain these observations, the discrepancy with the other experiments was not addressed. It can be proposed that these observations can be understood if we assume the presence of specific adsorbates. As shown by Bahn *et al.* [10], CO binds strongly to the gold chain, turns it into an insulator, introduces kinks in the wire, and the CO bonded gold chain has the lowest energy among all the structures investigated. This would suggest that CO, or another contaminant of similar nature, is present in the vacuum space. At a typical pressure of 10^{-5} Pa the probability of this mechanism is high.

In the Yanson's experiment [2] the distance between the peaks was reported to be large, 0.36 nm ($\pm$30). The larger value, and the rather large uncertainty, later turned out to result from the presence of He thermal exchange gas in the vacuum space. As was recently shown by Kolesnychenko *et al.* [17], adsorbed He gas has an unexpectedly large influence on the work function of metal surfaces. This introduces an error in the calibration of the displacement of the MCBJ and STM, when using the exponential tunnelling dependence. More recently,

Untiedt *et al.* [18] have combined several calibration techniques to obtain a more reliable value for the inter-peak distance in the length histograms, and the value obtained for Au, 0.26 ± 0.02 nm, is in excellent agreement with the calculated Au-Au distance in the chain [6, 7, 19, 20, 21, 22, 23].

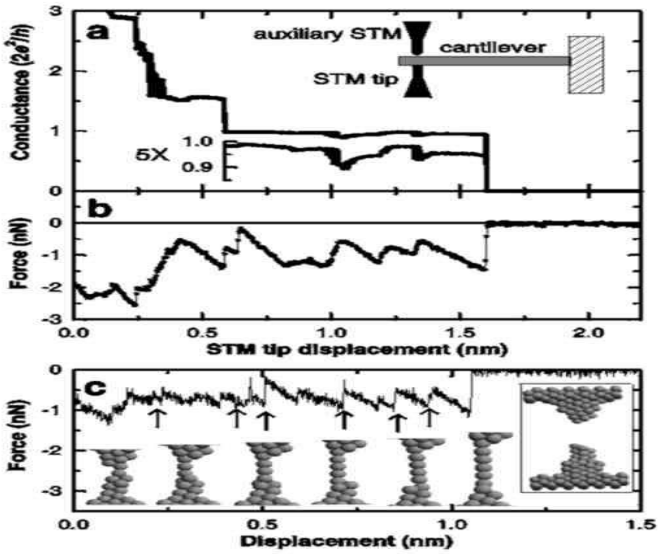

Figure 3.6: Simulation conductance (a) and force (b) measurements during chain formation and breaking. The conductance on the last plateau is shown on an expanded scale to illustrate small variation in the conductance. The inset shows a schematic drawing of the experimental setup. (c) Calculated force evolution obtained from molecular dynamics simulations. The arrows indicate the point at which a new atom pops into chain and snapshots of the structure at these positions are shown. Taken from [23]

Rubio-Bollinger *et al.* [23], measured the force evolution simultaneously with the conductance while drawing out a chain of atoms at 4.2 K, see figure 3.6. They employed an auxiliary STM at the back of a cantilever beam, on which the sample was mounted, in order to detect the deflection, and there with the force on the sample. An example of such a measurement is shown in figure 3.6, where the contact is stretched at a constant speed of 0.5 nm/s. The force shows a saw-tooth-like pattern corresponding to elastic deformation stages interrupted by sudden force relaxations. The conductance on the last plateau remains nearly

constant and just below 1 G_0, but note that the force jumps are accompanied with simultaneous jumps in the conductance with a magnitude of only a small fraction of G_0. In each measurement, the largest force on the last conductance plateau is reached at the end, as expected. For a series of 200 experiments this final breaking force shows a narrowly peaked distribution, centered at 1.5 nN, with a standard deviation of only 0.2 nN. The break force was found to be independent of the chain length. The force is considerably larger than the force required to break individual bonds in bulk gold, which is estimated at only $0.8 - 0.9$ nN, and this large force agrees very well with theory.

It was at first sight surprising to find that the slopes of the force as a function of displacement are nearly constant in experiment. One would expect a smaller force constant for longer chains. This observation is explained by the fact that the chain is unusually stiff. The bonds are much stronger than bulk bonds, and the largest elastic deformation takes place in the banks next to the chain. The calculated deformation of the banks amounts to $0.5 - 1.0$ nm, which agrees well with the offset observed in the return distance.

3.2 Computational calculations with pure gold atomic chain

Several molecular dynamics simulations have preceded those experiments which suggested the formation of chains. However, the effective potentials employed in these simulations were not regarded to be sufficiently reliable to be predictive for such exceptional atomic configurations. Nevertheless, in many cases the simulations agree with the observations, and they are very helpful in visualizing the mechanism by which the chains unfold from the banks. Full DFT molecular dynamics modelling of this process is still too demanding. More recently da Silva *et al.* [19], have used a method that forms a compromise between accuracy and computational efficiency, involving tight-binding molecular dynamics. The results for gold are generally consistent with the previously employed methods.

First-principles DFT molecular dynamics was used by Häkkinen *et al.* [24], by limiting the number of possible configurations. Taking a starting configuration of two atomic gold tips connected by two parallel two-atom long strands, the stretching of this double chain was seen to evolve into a four-atom long single atom chain via a bent chain structure.

In order to investigate the equilibrium structure, bond length and breaking force many model systems of moderate size have been considered, using first principles calculations. The structures considered are infinite chains, using periodic boundary conditions [21, 22, 25, 26], finite isolated chain sections [6, 21], or finite wires connected to an atomic base on either side [6, 20]. Sanchez-Portal *et al.* [6], have investigated all structures by various computational approximations and find only minor quantitative and no qualitative differences. All calculations agree on the equilibrium bond length, ranging only between 0.250 and 0.262 nm, and agree on the maximum bond distance at which the chain breaks, 0.28 - 0.30 nm. The break force is more sensitive to the type of approximations involved, ranging from 0.91 nN in Ref. [20] to 2.2 nN in Ref. [6]. Rubio-Bollinger *et al.* [23], made the most extensive analysis of the breaking force and obtained a force between 1.55 and 1.68 nN, in good agreement with the experimental value of 1.5 ± 0.3 nN.

Takayanagi *et al.* [20], demonstrated that a single-row gold atomic chain is modulated as it is stretched, like Peierls distortion [27, 28, 29]. A linear chain with four atom has a maximum restoring force of 0.91 nN at an average interatomic distance 0.31 nm. The interatomic distance of this chain reaches 0.345 nm but the conductance is approximately 0.4 G_0. The stretching chain changes its bonding nature from an atomic coupling state to a dimer coupling state around average interatomic distance 0.30 nm. Due to Peierls like distortion conductance decrease with stretching. They calculated the cohesive energy of both equally spaced chain and optimized chain. After d=0.29 nm dimerized structure is energetically favorable.

Torres *et al.* [22], examined theoretically the spontaneous thinning process of tip suspended nanowires and the structure and stability of monoatomic gold wires. They used thermodynamics, classical many-body force simulations, LDA

and GGA electronic calculations as well as *ab initio* simulations including the two tips. They argued that the wire thinning was well explained in terms of a thermodynamics tip suction driving migration of surface atoms from the wire to the tips. The monatomic wire become progressively stretch for the same reason. However, all calculations indicated that the stretched monatomic gold wire was unstable against the breaking, contrary to experiments. They tested the longitudinal stability by calculating the total energy changes when one interatomic spacing was extended from d to d^* fixing the total length of the wire. Wire was stable just around equilibrium value. They proposed some explanation for stability of monatomic gold wire seen in experiments. First one was weak electron correlations in bulk Au could became strong in stretched wires, due to poor coordination and large interatomic distance. Second was van der Walls interactions which are strong especially between blunt tip. Final one was heating or charging of wire due to TEM electron beam.

Sanchez-Portal *et al.* [6], found for the optimized geometry a planar zigzag structure with two atoms per unit cell. The zigzag deformation was even found for free standing wire sections and the origin was proposed to be related to a reduction in the transverse kinetic energy for the electrons due to the increased effective wire width. The relative stability of zigzag chain can be understood in comparison between the band structure of the linear chain and zigzag chain. In the linear chain, the overlap between the filled d states broadens the d bands until they reach the Fermi level, destabilizing the wire with their associated high density of states. For the same wire length, the zigzag configuration allows a larger bond distance; that brings back the d bands below the Fermi level and leaves the a single s band crossing it. The chain is stretched to a linear configuration only for bond lengths above about 0.275 nm, shortly before breaking. The zigzag structure is confirmed in the work of Refs. [10, 21]. On the other hand, Häkkinen *et al.* [24], find for a four atom chain between two tips that, before the chain is fully stretched, it assumes a bent configuration, that appears to be lower in energy than the zigzag conformation.

For a linear chain with a single half-filled conduction band a Peierls distortion towards a string of dimers is generally expected to occur. The majority of the

calculations suggest that this dimerization only sets in just before stretching to the point of breaking. The variation in bond lengths observed for a four-atom chain by Häkkinen *et al.* [9], that was argued to be related to a Peierls distortion may also be due to end effects [20]. De Maria and Springborg [21], took into account the relativistic effects on the band structure. But general picture was not change. Moreover they demonstrated that finite chains was very similar to infinite chains. They provided fairly general arguments that the half-filled band for this chain system should lead to dimerization when the bond length becomes larger than 0.29 nm. They argued that tendency towards dimerization largely was determined by the size of electron phonon coupling. This implies that strength of this tendency was independent of the unit cell length. Below 0.27 nm a second band was found to cross the Fermi level and the σ orbital becomes partially depleted. Since the σ orbital is no longer half filled the driving mechanism to dimerization is suppressed. A second band crossing the Fermi level for short distances was also found for linear chains in Ref. [6]. However, in their calculations it is removed by the zigzag deformation. The presence of a second conduction band should be visible in the conductance. Calculations of the conductance by other groups consistently find a conductance equal to 1 G_0 or slightly below, in agreement with the experiments.

The atomic chain configuration is clearly a meta-stable structure. Bahn *et al.* [10], calculated the time to break a chain for various temperatures by the effective medium theory (EMT) molecular dynamics method. He found that the chains would be unstable on a time scale of nanoseconds at room temperature. The barrier to breaking is only about 0.03 eV, with an attempt frequency of $5.10^{11}\mathrm{s}^{-1}$. Only higher temperature break times could be obtained in the time span accessible by these calculations. The mean time to breaking at 200 K is found to be ~ 0.1 ns, while extrapolation of the numbers obtained gives a lifetime of hours or even days at 4.2 K. The lack of predicted long time stability poses a second challenge to understanding of the room-temperature TEM results.

3.3 Computational calculations with impurities

As mentioned before in experiments interatomic distance between gold atoms were found in a range between 0.26 to 0.5 nm. In computational studies with pure gold chain, the chain was unstable much before than unusual long interatomic distance obtained in experiments. The presence of chemical species, such as CO and O, C, H may resolve the problem. Bahn *et al.* [10], investigated the chemical properties of single atomic gold chain by using DFT. The nanowire was shown to be chemically active with strong chemisorption of oxygen atoms and carbon monoxide. Due to low coordination number, quantum size effects and strains, gold nanowires are chemically active, in contrast to surfaces and bulk gold. The dependence on coordination number related to changes the energy of metal d states. They argued that the chemisorption energy strongly depended on the height of the unit cell. As the chain stretched chemisorption energy increased significantly for CO. The chemisorption of CO leaded to opening a gap in the electronic structure so conductance reduced. However, a chain with oxygen atoms inserted between the Au atoms would, surprisingly, still be conducting, with a single conductance channel. They argued that oxygen-gold chains were conducting and stable towards breaking because of thermal fluctuations the pure gold chain and they had gold-gold distance in the same range as the long chain lengths observed in experiments.

A similar result was obtained by Häkkinen *et al.* [9], for the insertion of methylthiol, SCH_3, into a gold chain. They used a four atom nanowire with two pyramidal tips both ends of the wire. They started equally distance nanowire and relaxed it with fixing the some part of the tips. The dimerization occurred in the middle part of wire. Energy gap increased near E_F from 0.194 eV in the equdistance wire to 0.216 eV in dimerized one. The calculated conductance of dimerized wire was 0.58 G_0. With binding of SCH_3 in different place of dimerized wire, the dimerization of the interior wire gold atom was removed. Both electrical and structural properties changed. Conductivity of dimerized wire increased to 0.82 and 0.88 G_0 for two different configuration. Increasing of conductance can be explained with examination of potential profile governing the propagation of

the electron through the wire. In the dimerized wire, unequal spacing between atoms and reduced overlapping between the electronic states of the inner part of wire and tips cause to reducing of conductance. They also argued that structure and conductance of wire was sensitive to small variations in the spacing between electrodes. So such sensitivity to small variations in the interelectrode distance, as well as the variation of interatomic distance in the wire due to thermal effects, may account for significant variations in the measured conductance at the final stage of elongation and consequently may affect the correlation between conductance and measured tip to tip distance.

Legoas *et al.* [11], experimentally observed the formation of stable linear gold atom chains and get direct real space information on atomic position and bond length. They obtained a length histogram. Bond length covered the whole range from 0.288 to 0.48 nm. To explain the origin of large Au-Au interatomic distance, they carried out the *ab initio* density functional theory geometrical optimization calculations for gold clusters assuming the presence of C impurity. Their result showed that existence of $0.40 - 0.50$ nm distance could be explained by presence of C_2 impurity. However, the bond-lengths above could be explained by a mixture of clean stressed bonds and incorporating a single C atom.

Skorodumova *et al.* [12], studied the unusual structural stability of monatomic gold wires by using first principles quantum mechanical calculations. They show that undetected light atoms, in particular hydrogen, stabilize the experimentally observed structures, which would be unstable in pure gold wires. They argued that this enhanced cohesion was due to partial charge transfer from gold to hydrogen. The studied chain both with and without supported tip. They obtained the very similar results. They also studied reactivity of gold surface and bulk gold. They checked the stability of Au-H chain by increasing the temperature from T=0 K up to T=300 K. Chain remained intact. They also studied the Au-O and Au-C chain. C and O were also stabilized the chain. They calculated the conductance by shifting the chemical potential at the one side and they found that Au-H were conducting.

Novaes *et al.* [13], studied a realistic Au atomic chain nanowire contaminated

by H, N, C, S, O and B. They argued previous studies about contaminated nanowire were unrealistic. In [12], they not only used a quite unrealistic model for nanowire but also they constructed a system with too H many system. But in their study nanowires was under stress. In [11], authors used free clusters and their clusters were not under tension. Experimental distance were taken under stress, so their calculation could be meaningful under stress. Novaes *et al.* [13], used a realistic model and small number of impurity. They argued that either in completely pure or contaminated wire, the Au-Au bonds broke at distance of 0.30 and 0.31 nm. Distance 0.36 ± 0.02 nm could be explained only by impurities and their candidate was H. Distance $\sim$ 0.48 nm could be explained by S. In contaminated wire, the overall effect of the impurities was to modify the stiffness of the bonds. The Au-impurity-Au and their adjoint Au-Au bonds were much stiffer than Au-Au bonds in pure wire.

3.4 Origin of the chain formation of metal atoms

As saying before nanowires of gold atoms spontaneously evolve into chains of single atoms, which are surprisingly stable. They form metallic wires with a nearly ideal quantum value of conductance $G = \frac{2e^2}{\hbar}$, and are able to sustain enormous current density. Various numerical calculations on these chains have been presented, in both regular and distorted configurations. All the experiments and calculations explained above are done for Au. Au appears to be favorable for chain formation while Ag and Cu do not. This leads to Bahn and Jacobsen *et al.* [25] and Smit *et al.* [30], to investigated the mechanism behind this phenomenon. Bahn *et al.* [25], by using molecular dynamics simulations investigated the several metals (Ni, Pd, Pt, Cu, Ag and Au). They showed that tendency for chain formation at low temperature is strongest for Au and Pt. They claimed that this could be understood based on the fact that for these two metals the bonds in low coordinated structures such as chain are very strong relative to bulk bond as confirmed by DFT calculations. Smit *et al.* [30], proposed that the higher stability of the linear monatomic gold wire suspended between electrodes, over Ag and Cu which have a similar d band electronic structure, was attributed

to s-d competition caused by relativistic effects. The contraction of s electron distribution for a 5th row element is much more significant than that for 3rd and 4th row atoms. This contraction reduces the energy of s electron and increase its occupation number at the expense of d electrons. Since the top of the d bands consists of states with anti bonding character that are now partially depleted, the d bonds becomes stronger. While the d electrons thus tend to compress the lattice, the s electrons exert an opposing Fermi pressure. At low dimensions, the spilling out of the s electron into vacuum relieves its expensive Fermi pressure and leaves 5d contractive pressure uncompensated thereby allowing a contraction of nearest-neighbor distance with a strengthened interatomic bonding.

Chapter 4

METAL NANOWIRES

4.1 Introduction

The miniaturization of the electronic components is of great importance in the development and improvement of new devices. Although the laws of nature are the same for macroscopic and mesoscopic systems, the miniaturization process is approaching the limit where the quantum behavior of matter starts to play an important role.

If the size of the system under consideration is only a few nanometers, the atomic character of matter emerges and it cannot be considered as a continuum. The regime of quantum behavior is also reached if one of the spatial dimensions of the system is comparable to Fermi wavelength of the conducting electrons. Then, the confinement splits the continuous electronic band in this direction into a set of discrete levels. In both cases, the behavior of the system changes from what is expected from the macroscopic case. In metallic nanowires the Fermi wavelength is of the same order of magnitude as the atomic distance, and both atomic and electronic discrete character compete and/or couple, determining the properties of the nanowires.

In this chapter, properties of one atom thick infinite nanowires are investigated from first principles. Electronic structure calculations based on the density functional theory are reported.

The organization of the chapter is as follows. In sec 4.2 computational details are presented. In sec 4.3.1 results for zigzag and linear wires are presented and six different metals (Au, Al, Ag, Cu, Pt and Na) are investigated. In sec 4.3.2 dimerization is discussed for these monatomic nanowires.

4.2 Computational Details

Pseudopotential plane wave [31] method is used in these DFT total energy calculations. The exchange-correlation effects are described by the generalized gradient approximation (GGA) by using PERDEW-WANG 91 [32] formulation. The interaction of the valence electrons with the ionic cores is modelled by ultrasoft Vanderbilt [33] pseudopotentials. Because of the periodic boundary condition, the supercell [34] approximation is used. The chain is placed in a large tetragonal cell. The axis of the wire is taken along the z axis. In the linear chain 12 Å cell dimension along x and y axis is sufficient to eliminate the interaction between the wire and its periodic images. The zigzag chains are treated in a supercell with the lattice constant of 14 Å perpendicular to chain axis. The Brillouin zone (BZ) integration is performed within Monkhorst-Pack [35] scheme. In order to describe the properties of nanowires correctly, the special k-points in the wire direction have to be dense enough. Different k-meshes are used for different metals. Number of the k-points are increased until a total energy convergence better than computational error range. The forces are given by the Hellmann-Feynmann theorem. The wavefunctions are expanded in the plane waves up to a cutoff 400 eV. In order to treat the partial occupancy around the Fermi level of metallic system, the Fermi smearing of 0.08 eV is used in the integrations. The convergence with respect to energy cut off and k-points are tested for each elements to obtain accurate energies and forces. Energies and forces along the one direction have converged within 10^{-4} eV/atom and 10^{-3} eV/Å per atom respectively.

4.3 Results

4.3.1 Infinite linear and zigzag wires

Chain nanowires of six different metals (Au, Al, Ag, Cu, Pt and Na) are investigated from first principles. The studied structures are constrained to be linear and planar zigzag. Total energy per atom is obtained by fixing both the shape and the dimension of the cell but optimizing the all atomic coordinates. For several different fixed chain lengths, total energy is calculated. The linear chain contains one atom per unit cell and zigzag chain contains two atoms. However, linear structure with two atom per unit cell is used to compare with zigzag one in energy band calculations. Figure 4.1 shows the cohesive energies of monatomic

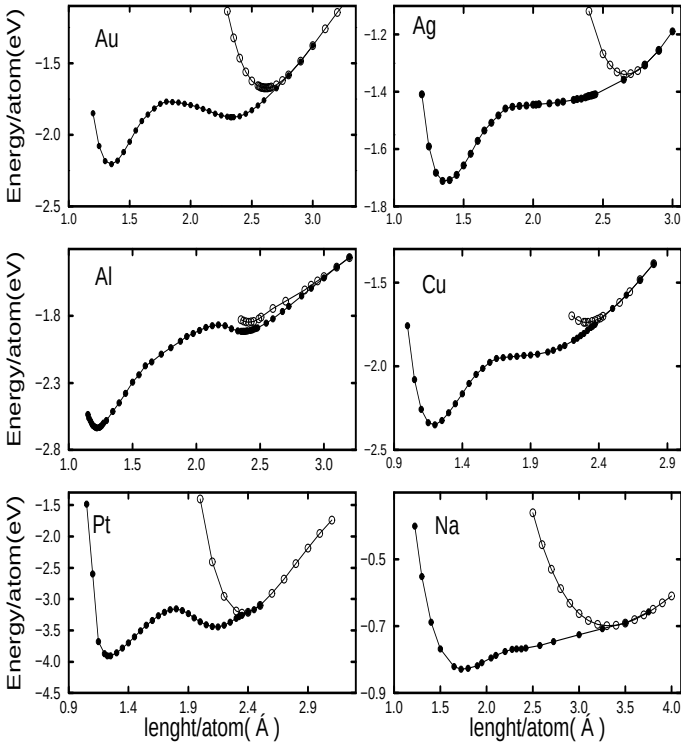

Figure 4.1: The calculated cohesive energy of infinite Au, Ag, Al, Cu, Pt and Na with linear structure (open circles) and zigzag structure (solid circles)

wires with planar zigzag and linear structure, as a function of the wire length,

for six different elements. The lengths are given as length per atom(s). It is the half of the cell parameter in z-direction for chain containing two atom per unit cell and it is equal to cell parameter in chains having one atom per unit cell in chain direction. Hence, it corresponds to the interatomic bond distance for linear chain containing one atom per unit cell. It is obvious that zigzag structure is more energetically favorable than linear one. Zigzag structure of Au [36, 37], Al and Pt have two minima. Structures of both minima are more stable than a linear structure, even before the linear structure reaches its optimum bond length. Zigzag and linear structure energy curves of Al begin to join after an interatomic distance of 3 Å. The situation is not different for other elements: zigzag structure is more stable than linear structure. Of course, relative stability of different atomic chains is not the same. It depends on element. By investigation of cohesive energy curves, energy band diagrams and charge density profiles of different atomic chain, one can obtain origin of stability of zigzag structure over linear one, and also explain why chain of some elements have high tendency to form chain. If one investigates Figure 4.1, it can be seen that Pt has the high cohesive energy for both zigzag and linear structure. These energies, bond length and bond angles are 3.40 eV, 2.35 Å and 180 for linear wire, 4.08 eV, 2.66 Å and 56.1 for zigzag1 (z1) structure and 3.62 eV, 2.37 Å and 130.2 for zigzag2 (z2) structure. Unlike Pt, both zigzag chain and linear chains of Na are only weakly binded. This can be understood from the fact that Na is free electron like metal. Energy differences between two zigzag minima and the barrier height of local minima are 0.33 and 0.11 eV for Au, 0.72 and 0.05 eV for Al and 0.46 and 0.28 eV for Pt. The system must over come this barrier to go to the most stable local zigzag structure. Therefore, local minimum (second zigzag structure) of the Pt is the most stable minimum. Cohesive energy curves of Au, Pt, Cu and Ag [38] have similar shape expect second zigzag minima in Au and Pt. Notice that the angle in global minima in zigzag structures are roughly similar to each other, slightly less than 60^o. Table 4.1 summarizes the information related to Figure 4.1.

In Figure 4.2, tension of the six studied system are shown. This is the derivative of the energy plot in Figure 4.1 and corresponds to applied force on the wire to keep the wire at that specific length. The zeros of the tension correspond to

Table 4.1: Comparison of calculated structural parameters and cohesive energy, E_C, for linear and zigzag structures of different elements. The nearest neighbor distance, d, and binding energy, E_C, are calculated for the optimized bulk crystals. s and α are the half of the supercell containing two atoms and zigzag bond angle respectively.

Atom	Structure	d (Å)	s (Å)	$\alpha(^\circ)$	E_C (eV)
Au	linear	2.615	2.615	180	1.67
	zigzag1	2.75	1.35	58.8	2.20
	zigzag2	2.57	2.335	130.6	1.87
	bulk	2.95			3.21
	dimer	2.53			1.29
Ag	linear	2.67	2.67	180	1.34
	zigzag	2.80	1.35	57.7	1.71
	bulk	2.93			2.76
	dimer	2.58			1.06
Al	linear	2.41	2.41	180	1.87
	zigzag1	2.68	1.22	54.2	2.64
	zigzag2	2.52	2.37	140.3	1.92
	bulk	2.8			3.77
	dimer	2.66			0.86
Cu	linear	2.3	2.3	180	1.74
	zigzag	2.41	1.2	59.7	2.36
	bulk	2.58			3.76
	dimer	2.22			1.334
Pt	linear	2.35	2.35	180	3.23
	zigzag1	2.66	1.25	56.1	3.91
	zigzag2	2.37	2.15	130.2	3.45
	bulk	2.81			6.0
	dimer	2.33			1.96
Na	linear	3.3	3.3	180	0.70
	zigzag	3.60	1.725	57.4	0.83
	bulk	3.53			1.28
	dimer	3.07			0.59

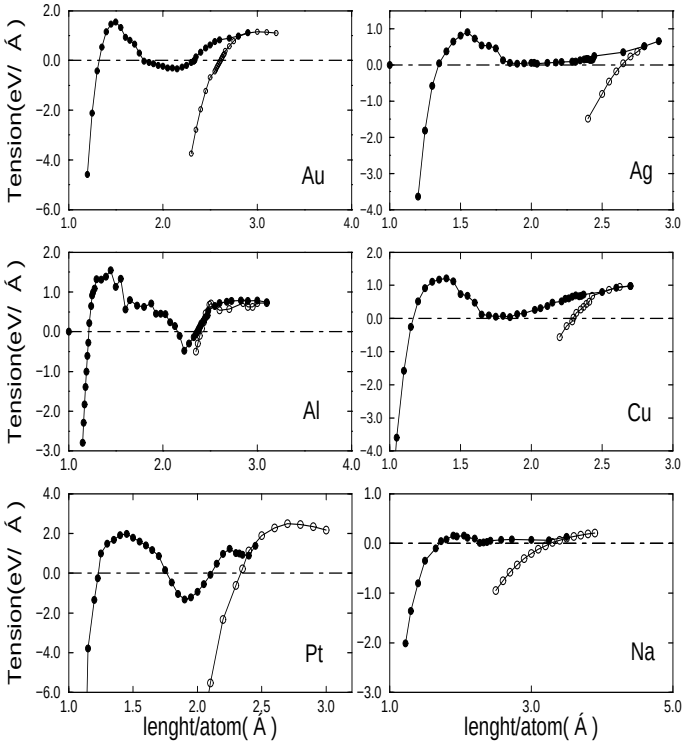

Figure 4.2: Tension versus length per atom of Au, Ag, Al, Cu, Pt and Na zigzag and linear wires. Open (closed) circles show linear (zigzag) wire.

minima or maxima of the energy, and positive (negative) slopes of the tension corresponds to stable (unstable) configurations relative to changes in strain or lattice constant. When a maximum of tension is reach with increasing strain, this correspond to maximum tension that can be applied to a wire before it breaks. The elongation force is defined as the force opposing the lengthening of the wire due to a tension. When it is negative, the elongation force would like to shorten the wire, whereas a positive elongation force without a counterbalancing force (tension) lead to spontaneous elongation. Naturally, the force vanishes at the minimum energy and is negative for larger distance. For very large distances, force should approach to zero.

Figure 4.3 shows the stress along the chain axis. One can obtain the tendency of chains to return equilibrium structure from this figure. As seen from this Figure, Pt, Au and Al have greater stress value. This means that they have

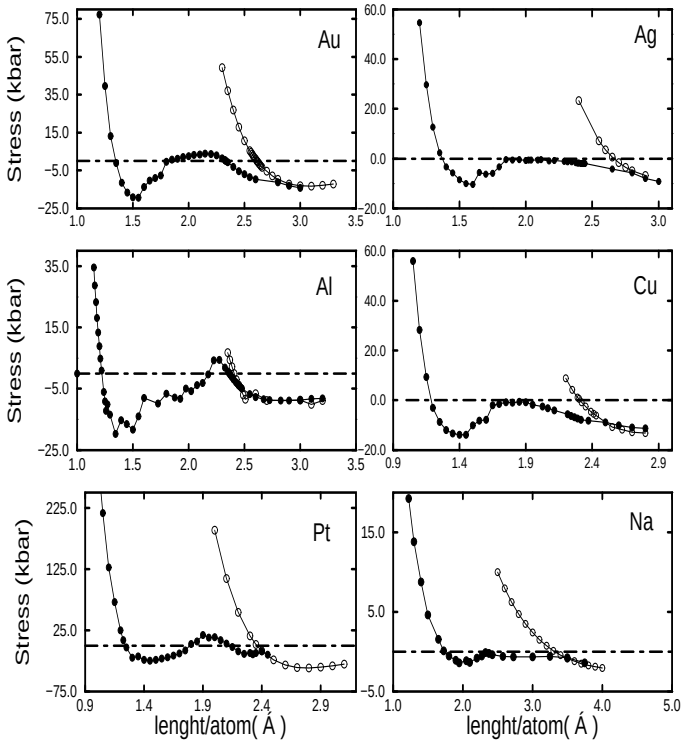

Figure 4.3: Stress versus length per atom of Au, Ag, Al, Cu, Pt and Na zigzag and linear wires. Open (closed) circles show linear (zigzag) wire.

high tendency to return equilibrium structure of both linear and zigzag wires. Obviously, since these chains are quasi one dimensional systems, tension and stress have opposite sign.

Figure 4.2 gives clues about the stabilities [39] of wires. As seen from Figure 4.2, the force to break the wire is the highest in Pt. Au and Al also have the greater breaking forces than Ag, Cu and Na. From the tension breaking plot, it is seen that if one stretches the second stable Au zigzag (z2) it smoothly changes to the stable linear chain. Except for Al and Pt, this property is observed in all other studied wires. In Al wires, zigzag wire curve oscillates around linear curve.

4.3.2 Instabilities in linear wires

The regular chain structure in one dimension with a partial filled band will never be stable, since one always find a more suitable structure, such as a dimerized structure. It is so called Peierls distortion [27, 28]. In these phenomena, a band alternation occurs in the wire and wire changes from a conductor to an insulator. Peierls distortion is investigated as stretching the wire. In Figure 4.1, bond lengths between nearest neighbors are all the same in both linear and zigzag structures. It can be asked whether this distortion occurs while stretching the wire or not. Four atom unit cell is used for all linear structures to investigated the dimerization. Figure 4.4 shows the cohesive energy with respect to lattice

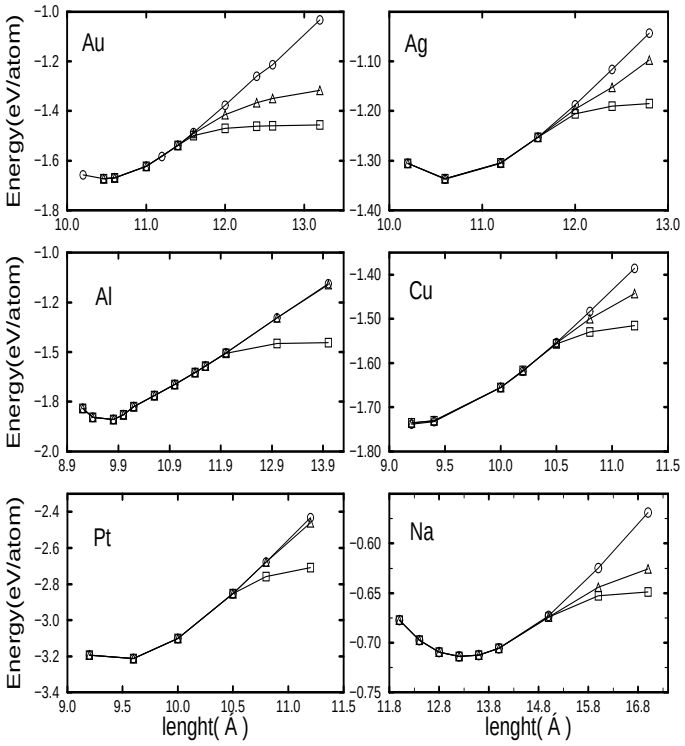

Figure 4.4: Cohesive energy per atom with respect to total lattice constant. Open circles, triangle and square are used for equally space, dimerized and breaking wires respectively.

constant in wire direction. Open circle, triangle and square are used for equally spaced, dimerized and breaking wires respectively. In dimerized wire, there is

a bond alternation. Two different bond length exist. One is the interatomic distance in dimer and other is dimer-dimer distance. In breaking structure, one of the bond is very large relative to others which are in range around equilibrium distance of individual wire. Dimerized and breaking structures are obtained by moving the second and third atom of wire in opposite direction in a small amount. The systems are then allowed to relax. It is seen from Figure 4.4 that the equally spaced structure is not favorable energetically after a certain lattice constant. Energy gain upon in dimerized and breaking wire increase with lattice constant after this lattice constant. Energy gain is highest in Au with increasing lattice constant. In Al, dimerization is not occur [40, 41] until interatomic distances are very large. However, breaking wire structure favorable at an interatomic distance larger than 3 Å. In Pt linear wire, breaking wire is observed firstly. Splitting in energy curve occurs when wire is stretched about 1 Å from equilibrium

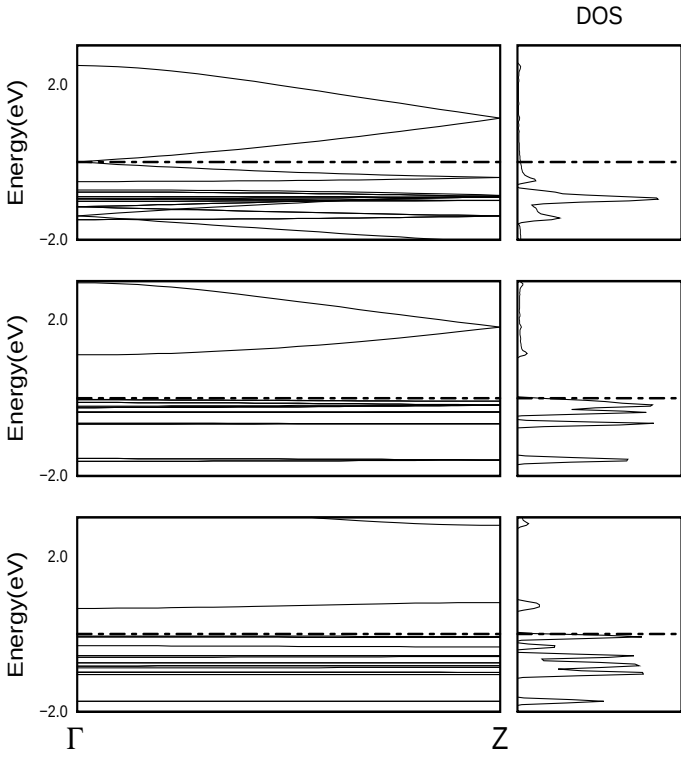

Figure 4.5: Energy band structure of (a) equally space, (b) dimerized, (c) and breaking structures.

lattice constant (0.25 Å per bond). When dimerization occurs, wire becomes an insulator. Figure 4.5 shows the energy band structure of Au linear chain with a lattice constant 13.2 Å for equally space, dimerized and breaking wire. As seen from the band diagram, there is a band crossing the Fermi level in equally spaced structure and a band gap is observed in the dimerized and breaking wire. Notice that d bands are flat structures. This shows that there are non-interacting dimers in the dimerized wire. Dimerization begins to be observed from the inflection point of energy curve. This inflection point can be seen from Figure 4.4 if one investigates that curve at which wire begin to deviate from the equally spaced structure. The bond lengths in dimers vary. It approaches equilibrium dimer bond length when distance between the dimers are far enough to eliminate interaction between them. Dimerized chain curve begins to become flat after that distance and total energy of the system can be approximated by the sum of the dimer energies. As pointed out before, one of the bond length is very large relative the others in breaking wire. So it can be argued that wire break at this bond. In this structure, the energy gain is larger than the energy loss due to breaking of a bond. In dimerized structure, more bonds must be broken. So, the energy gain is lower than breaking wire having the same lattice constant with the dimerized wire. It can be estiminated that the energy of broken bond by taking the differences of equilibrium structure energy and energy of lattice constant at which flatting of energy curve begin from the breaking structure. Table 4.2 shows

Table 4.2: Comparison of calculated breaking point, breaking force, stress at breaking point and broken bond energy in breaking wire.

Atom	breaking point (Å)	Breaking force (eV/Å)	stress(kbar)	E_{bond} (eV)
Au	2.9	1.11	-12.12	0.19
Ag	2.9	0.66	-6.85	0.13
Al	3.0	0.72	-8.77	0.36
Cu	2.625	0.95	-11.82	0.20
Pt	2.625	2.48	-33.5	0.52
Na	3.75	0.18	-1.59	0.07

breaking point, breaking force, stress at breaking point and broken bond energy in breaking wire. It is easily seen that breaking force at breaking point is the highest in Pt linear wire. The calculated breaking force for Au is consistent with the breaking force obtained in experiment [23]. Breaking force is the smallest in Na linear wire.

4.3.3 Electronic structures

Figures 4.6 to 4.11 show the energy band structures of the studied structures. A comparative analysis of these structures provides further insight into stability and electronic properties of wires. First observation can be about metallicity of wires. As seen from band structures, all the wires in both structure are metallic. This means that at least one band crosses the Fermi level. Number of band

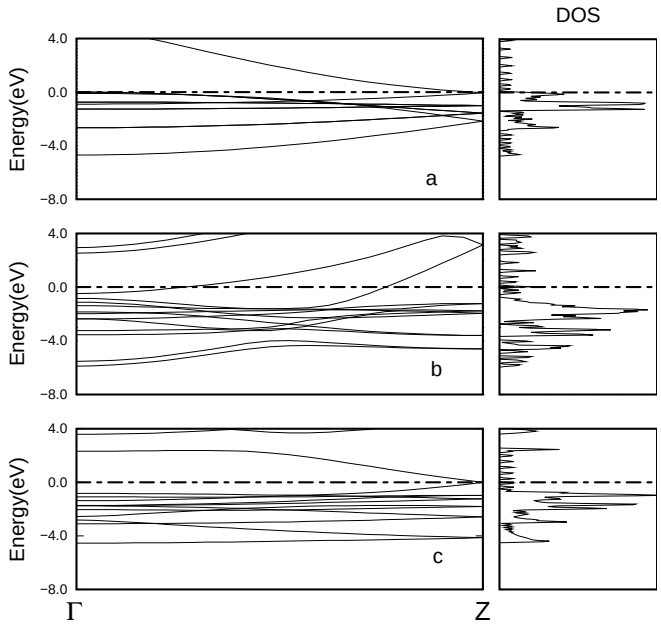

Figure 4.6: Energy band structure of Au. (a) Linear structure L; (b) zigzag1, z1; (c) zigzag2, z2. Bands of L structure are zone folded for the sake of the comparison with zigzag structures. Zero of energy is taken at Fermi level.

crossing is one in Au, Ag, Na and Cu [42] linear wires, except in Pt linear wire

which is four and in Al linear wire which is two. Number of bands which cross the

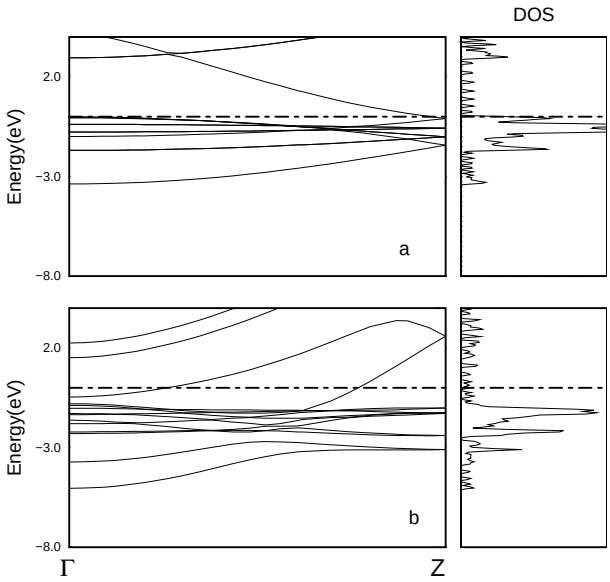

Figure 4.7: Energy band structure of Cu. (a) Linear structure L; (b) zigzag structure z. Bands of L structure are zone folded for the sake of the comparison with zigzag structures. Zero of energy is taken at Fermi level.

Fermi level is critical for quantum ballistic conductance and stability of nanowires. Under ideal conditions, the conductance is determined by the number of bands crossing the Fermi level, being G_0 per band. In Cu and Au linear wires, this band has mainly s character. However, in these wires, d bands reach the Fermi level close the Γ point. So s band has not purely s character. In Ag linear wire, d bands are far below the Fermi level. So crossing band is predominately s character. The transition from linear wire to zigzag one bring back d bands below the Fermi level. This transition also increases the number of conducting band. In Cu, Au, and Pt linear wires, the overlap between the filled d states broadens the d bands until they reach the Fermi level, destabilizing the wire with their high density of states. The transition from linear wire to zigzag one lowers the density of states at the Fermi level and stabilizes the zigzag wire relative to linear structure. In z1 structure of Au and Al and z structure of Na, Cu and Ag, there are two bands crossing the Fermi level. Au, Ag and Cu have closed d shell. This d charge distribution is nearly spherical. However, Pt has an open

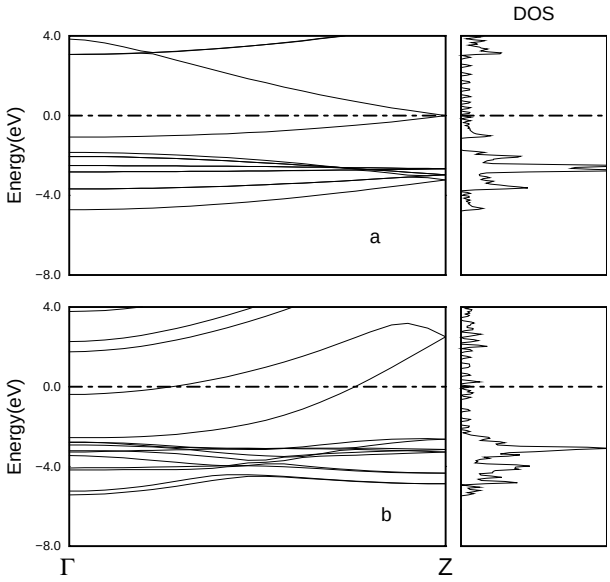

Figure 4.8: Energy band structure of Ag. (a) Linear structure L; (b) zigzag structure, z. Bands of L structure are zone folded for the sake of the comparison with zigzag structures. Zero of energy is taken at Fermi level.

d shell. d bands contribute both bonding and conduction. In linear Pt wire, d bands are degenerate. So there are four bands crossing the Fermi level. When linear Pt wire transforms to z1 structure, number of bands crossing the Fermi level increase to six. In z2 structure number of bands crossing the Fermi level are two. The overall shapes of the band structures of Au, Ag, Cu, and Pt wires are almost the same. In Al linear wire, because of the linear geometry, $3p_x$ and $3p_y$ are equivalent and give rise to doubly degenerate π band crossing the Fermi level. When wire transform from linear to zigzag geometry, the symmetry between $3p_x$ and $3p_y$ orbitals is broken and so the π band is split. This splitting can be seen from Figure 4.10. In z2 and z1 structure, number of crossing bands (it is 2) do not change upon linear-zigzag transformation.

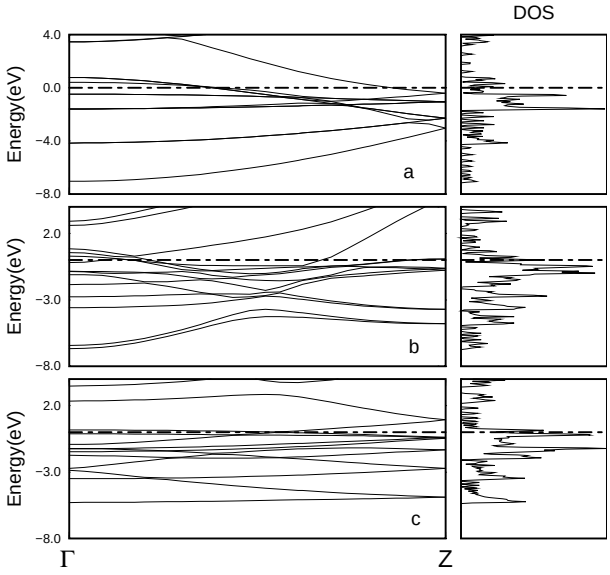

Figure 4.9: Energy band structure of Pt. (a) Linear structure L; (b) zigzag1, z1; (c) zigzag2, z2. Bands of L structure are zone folded for the sake of the comparison with zigzag structures. Zero of energy is taken at Fermi level.

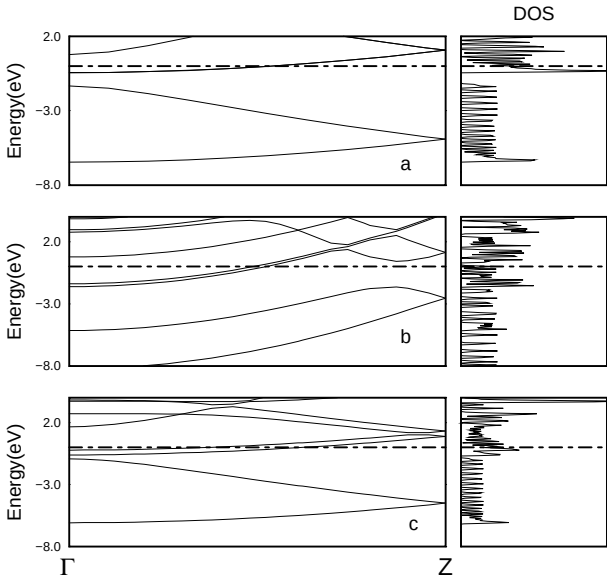

Figure 4.10: Energy band structure of Al. (a) Linear structure L; (b) zigzag1, z1; (c) zigzag2, z2. Bands of L structure are zone folded for the sake of the comparison with zigzag structures. Zero of energy is taken at Fermi level.

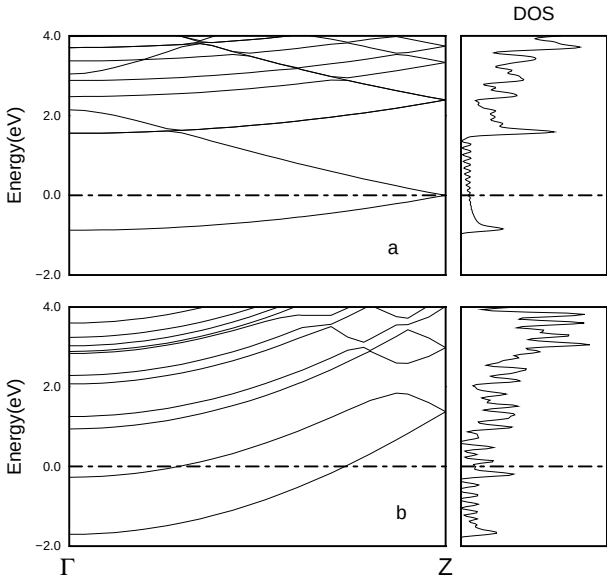

Figure 4.11: Energy band structure of Na.(a) Linear structure L; (b) zigzag structure, z. Bands of L structure are zone folded for the sake of the comparison with zigzag structures. Zero of energy is taken at Fermi level.

4.3.4 Charge density analysis

Figure 4.12 and 4.13 show the charge density contour plots of linear and zigzag structures of studied elements. The character of the bonding in wires is revealed by the analysis of electronic charge density. It can be easily seen that bonding in both linear and zigzag structure of the Au and Pt are not directional. Valence charge is delocalized. Like Au, Ag has a closed d shell and s valence orbital. In Ag wires, charge distribution is uniform. So bonding is not directional. Moreover Cu wires have also non-directional bond. In contrast, Al has directional bonds in both linear and zigzag structure. Al with valance states consisting $3s$ and $3p_{x,y,z}$ orbitals form directional bond. In z1 structure of Au, Pt and Al, bonding between second nearest neighbors become significant because they begin to close each other and overlapping between atomic orbitals increases. In this structure, the equilibrium configuration can be interpreted as two linear wires side by side but dislocated from each other in the longitudinal direction by the half of interatomic

distance. As seen from charge density plots, interaction between first nearest neighbor is low relative to second nearest neighbor (second relative to linear and z2 structure).

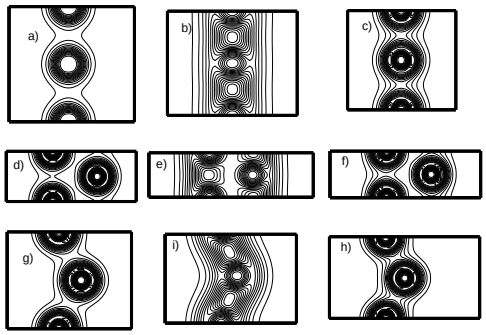

Figure 4.12: Charge density contour plots of linear in (a) and z1 in (d) and z2 in (g) of Au, linear in (b) and z1 in (e) and z2 in (i) of Al, of linear in (c) and z1 in (f) and z2 in (h) of Pt wires.

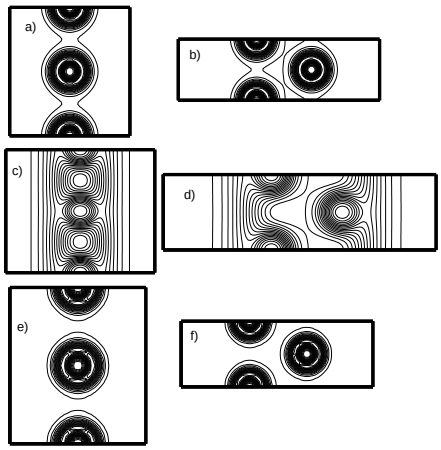

Figure 4.13: Charge density contour plots of linear in (a) and zigzag structure in (b) of Ag, linear in (c) and zigzag structure in (d) of Na and linear in (e) and zigzag structure in (f) of Cu wires.

Chapter 5

EFFECT OF IMPURITIES

5.1 Introduction

The atomic chains of gold atoms have been observed by an ultrahigh vacuum (UHV) electron microscopy [1]. The conductance of the chain has been measured during the withdrawal of the STM tip. That observation has demonstrated that a single [110] atomic row chain has had a conductance of 1 G_0. The single chain, which has formed in a [100] orientation, has interatomic spacing of 0.35-0.4 nm. It is a surprising observation, since normal nearest neighbor distance is 0.288 nm in bulk gold and is 0.254 nm in dimer. The origin of this large interatomic distance has been a serious and unresolved challenge for theoretical interpretation. In chapter 4, it is pointed out that the wires rupture before reaching such a long atomic distance.

It is known that gold is very noble, "chemically" inert and its surface has low reactivity. However, it has become clear over the last years that the situation is very different for small particles of gold which can be chemically active, and they are even considered catalytic materials. Several factors may play a role for the increased reactivity of small gold clusters. Small clusters have a large number of defects like steps and kinks which are more reactive than terrace atoms. Furthermore the presence of tensile strain-which in the case of the gold clusters

could come from the interface between the clusters and the supporting materials are also known to increase the chemical activity. Finally, for very small particles it is possible that direct quantum size effects could play a role for the reactivity. All of these factors (low coordination, strain, and quantum size effect) can be expected to be present to a large extent in gold wires: the coordination number in a perfect monatomic wire is around two, the chains are produced by mechanical stretching with significant strains, and the observed quantized conductance is a clear demonstration of quantum size effect. Gold wires can be therefore expected to have different chemical properties than bulk gold and its surface [10].

In this chapter, effects of H, H_2, and C absorptions on mechanical stability and electronic properties of gold monatomic wires are investigated.

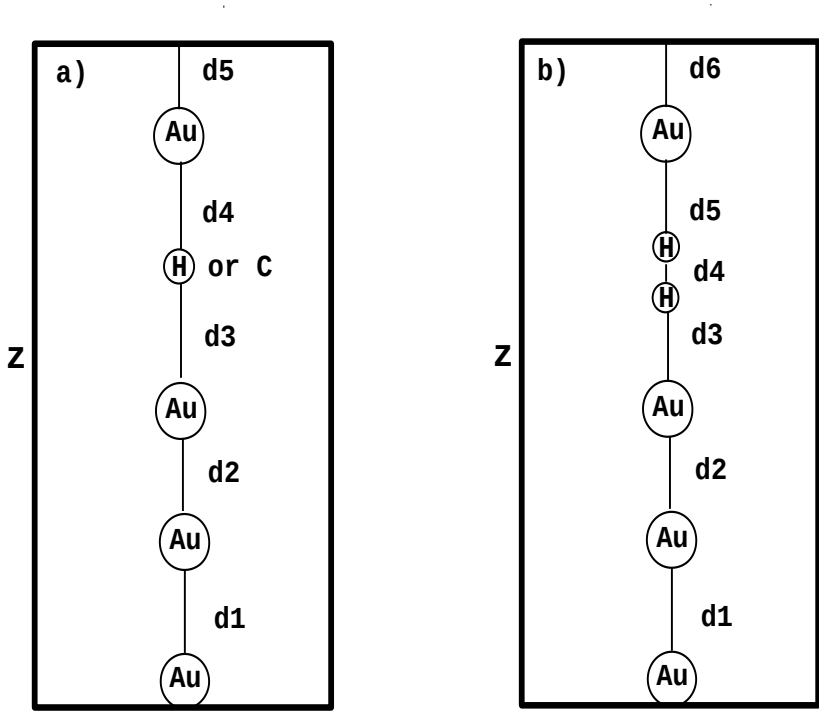

Figure 5.1: HOPT (contain H) and COPT (contain C) geometries in (a) and HMAOPT (contain H_2) geometry in (b). z is the lattice constant along the chain direction.

5.2 Results

In this chapter, supercells containing varying number of Au, H and C atom are used. Starting geometries are shown in Figure 5.1. In HOPT and COPT configurations H and C atoms are in chain and bond lengths are satisfy following equalities; d_1=d_2=d_5 and d_3=d_4. Distance of H and C atoms to Au is larger than 1.5 Å. Impurity is also placed very close the one of the Au atom and system is allowed to relax. After relaxation, impurity atom goes to middle of the bond. In H_2 case, molecule atoms are separated from each other. After relaxation of this system, H atoms form H_2 molecule in the middle of the bond.

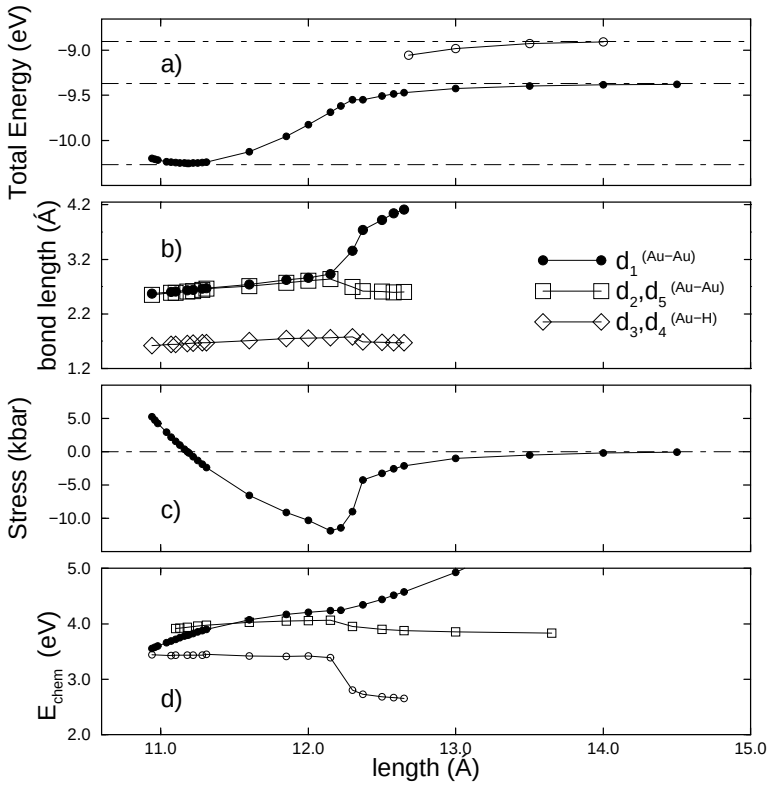

Figure 5.2: Total energy in (a), changing of bond lengths in (b), stress in (c) and chemisorption energy in (d) with respect to lattice constant (z) in HOPT structure. Open circle curve in (d) is drawn by taking the d_2 as a lattice parameter of pure gold chain in z-direction.

Figure 5.2 and 5.3 show the cohesive energy, stress, chemisorption energy and

changing of bond lengths with respect to lattice constant (z). These curves are obtained by varying the lattice constant and relaxing the all atomic positions until all forces vanishes. Equilibrium lattice constant and energies are 11.18 Å

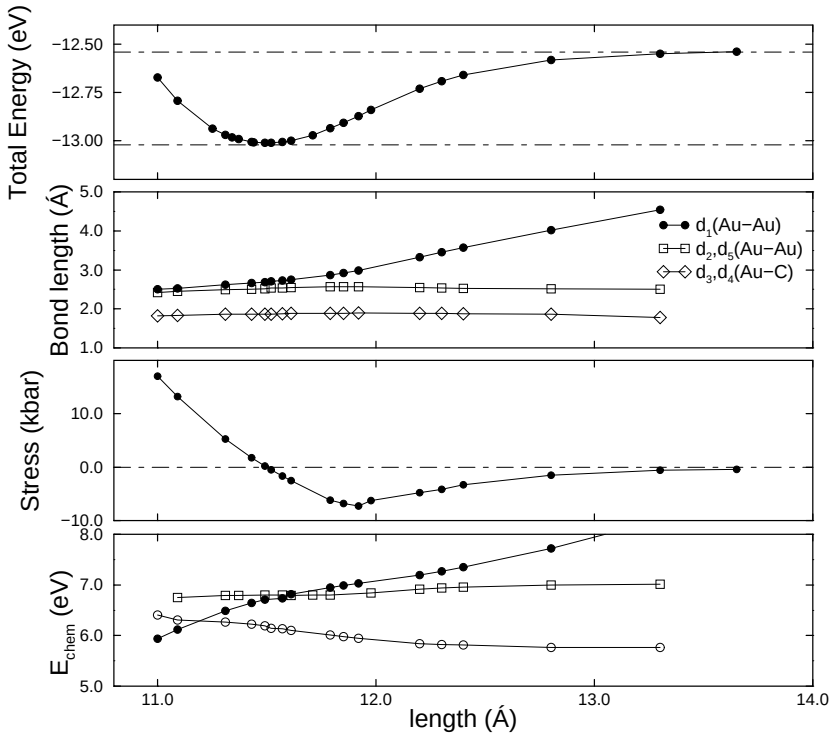

Figure 5.3: Total energy (a), stress (b), changing of bond lengths (c) and chemisorption energy (d) with respect to lattice constant (z) in COPT structure. Open circle curve in (d) is drawn by taking the d_2 as a lattice parameter of pure gold chain in z-direction.

and 10.27 eV for HOPT and 11.49 Å and 12.86 eV for COPT configuration. As seen from Figure 5.2 and 5.3 that when one stretch the HOPT wire, all bond lengths increase. In contrast to HOPT, the bond away from the C atom stretches much more than other bonds. C part is very rigid. In both configuration, breaking bond is far from the H and C. This means that presence of H and C modify the stiffness of the bonds. The Au-H-Au, Au-C-Au and their adjoint Au-Au bonds are much stiffer than the Au-Au bonds in clean nanowires. As a consequence, the wire tends to break in a pure Au-Au bond far from the H and C. This situation can be seen from the total charge density contour plots as shown in (a), (c), (e)

of Figure 5.4. In order to see charge transfer between the Au atom and impurity, difference charge densities are also calculated as follows

$$\rho_{diff} = \rho_{Au+impurity} - \rho_{chain\ without\ impurity} - \rho_{impurity} \tag{5.1}$$

Au-C-Au increase. In other words effective binding between the Au-Au atoms nearing the impurity increases. In COPT case, it can be seen that C also affects

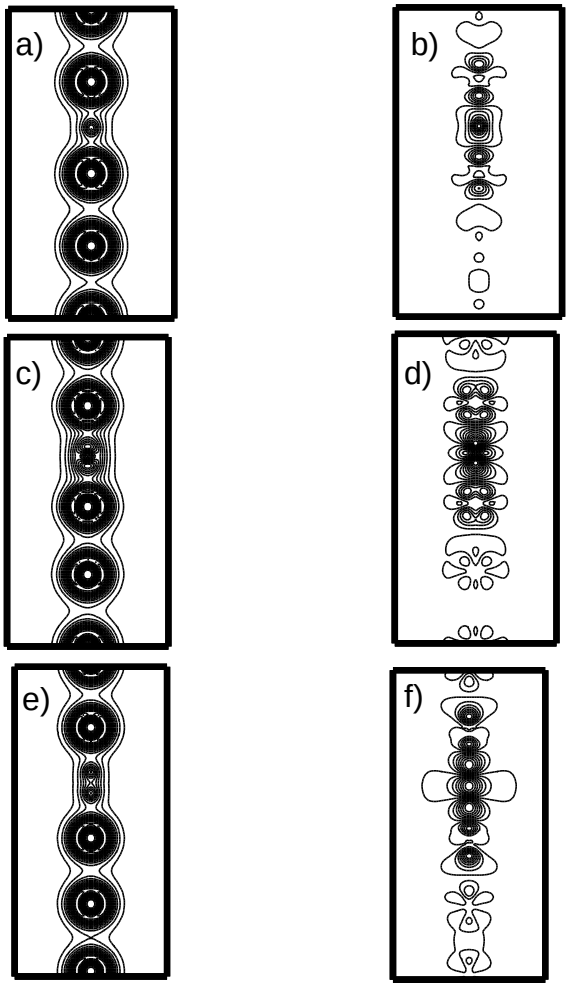

Figure 5.4: Charge density contour plots of in HOPT (a,b), COPT (c,d) and HMAOPT (e,f) structure. (b), (d) and (f) are the charge difference contour plots for HOPT, COPT and HMAOPT respectively. In HOPT and COPT configurations, there is a considerable charge transfer from Au to H, C. Hence stability of Au-H-Au and

the second nearest neighbor. So C part of the COPT is very rigid. This leads to

Table 5.1: Comparison of calculated breaking points, breaking forces, stressse at breaking points and broken bonds energy in breaking wire. d_a is Au-Au bond length nearing the impurity in equilibrium structure. d_b is the Au-impurity-Au bond length in equilibrium structure. E^c_{bond} is the broken bond energy of Au-Au bond away from the impurity. E^d_{bond} is the broken bond energy of Au-impurity bond.

system	d_a Å	d_b Å	breaking point Å	E^c_{bond} (eV)	E^d_{bond} (eV)
Au-H	2.61	3.32	3.1	0.87	1.34
Au-C	2.52	3.74	3.05	0.47	2.80
Au-H_2	2.59	4.36	2.2 (Au-H_2)	0.66	0.30

much more stretching of Au-Au bond far from the C under tension.

In total energy curve of HOPT, there is a small curve denoted by open circle. This curve is obtained for HOPT structure by constraining a broken Au-H bond. Comparison with HOPT having a broken Au-H bond shows that there is a energy loss due to breaking of Au-H bond. The situation is the same for COPT structure. If one breaks the Au-C, there is a energy loss. So breaking of Au-C do not energetically favorable as in the case of breaking of Au-H bond. The maximum Au-H and Au-C distances are around 1.78 Å and 1.9 Å respectively. As seen from Figure 5.2 and 5.3, after a certain lattice constant, curves begin to flat. This means that bond exactly disappears. Bond energies are calculated by using the same method described in chapter 4. The broken bond energies are 0.87 eV for HOPT and 0.47 eV for COPT. As seen from these calculated energies, broken bond energy is small in COPT structure relative to HOPT structure. This can be understood that C affect the second nearest neighbor. If one compares the broken bond energy of pure Au wire which is 0.21 eV and HOPT and COPT broken bond energy, absorption of H and C increase the stability of wire. Table 5.1 shows the breaking point, broken bond energy for Au-Au bond away from the impurity, broken bond energy for bond Au-impurity bond distance in Au-Au bond nearing the impurity in equilibrium and bond distance in Au-impurity-Au bond.

The situation is different in HMAOP structure. Wire breaks at Au-H_2 bond. If one investigate Figure 5.4, it is seen that the interaction between Au-H_2 is small due to binding in H_2 molecule. So, charge transfer is very small relative to HOPT and COPT structures. But, presence of H_2 molecule modifies the stiffness of bonds in chain. Energy of broken bond away from the H_2 impurity increases from 0.21 eV to 0.60 eV. It can be seen from Table 5.1 that Au-Au bond away from the H_2 impurity is much more stiff than Au-H_2 bond.

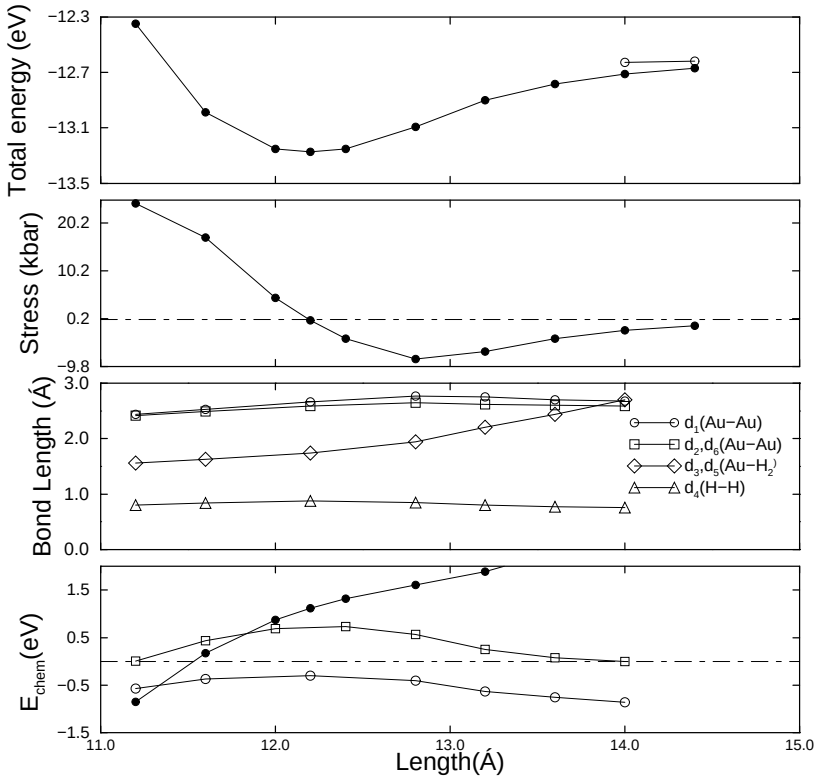

Figure 5.5: Total energy (a), stress (b), changing of bond lengths (c) and chemisorption energy (d) with respect to lattice constant (z) in HMAOPT structure. Open circle curve in (d) is drawn by taking average of d_1, d_2 and d_6 as a lattice parameter of pure gold chain in z-direction.

Comparison between these structures is also made by studying the chemisorption energies. Impurity chemisorption energy to the wire under tension is calculated by using following formula

$$E_{chem}(z) = E_{Au+impurity}(z) - E_{pure\ Au\ chain}(z) - E_{impurity}(z) \qquad (5.2)$$

where $E_{Au+impurity}(z)$ is the total energy of Au-impurity system. $E_{pure\ Au\ chain}(z)$ is the pure chain with length z, so that means it is under stress, and $E_{impurity}(z)$ is the impurity atom energy. $E_{chem}(z)$ is meaningful until the pure Au chain breaks.

Interaction energy of Au-impurity system is also calculated by using following formula

$$E_{int}(z) = E_{Au+impurity}(z) - E_{chain\ without\ impurity}(z) - E_{impurity}(z) \qquad (5.3)$$

where $E_{Au+impurity}(z)$ is the total energy of Au-impurity system. $E_{chain\ without\ impurity}(z)$ is calculated by removing the impurity atom. Resulting chain is not allowed to relax. $E_{impurity}(z)$ is the impurity atom energy.

Binding energy of these Au-impurity system is calculated by using following formula

$$E_{binding}(z) = E_{Au+impurity}(z) - E_{chain\ without\ impurity}(z^*) - E_{impurity}(z) \qquad (5.4)$$

where $E_{Au+impurity}(z)$ is the total energy of Au-impurity system. z^* is defined as lattice constant along the chain axis, as using d_1 (bond nearing the impurity) as the interatomic distance in pure equally spaced Au chain for HOPT and COPT geometries and average of the d_1, d_2 and d_6 (These are shown in Figure 5.1) for HMAOPT structures. So this $E_{binding}$ gives the binding energy of the impurity atom with respect to the optimum Au linear chain. In Figures 5.2, 5.3 and 5.5, chemisorption energy, interaction energy and binding energy are shown by solid circles, open square and open circles, respectively. As easily seen that chemisorption energy of C is the highest. In HMAOPT structure, there is a small chemisorption and interaction energy. However, binding energy is negative. This means that there is no binding, see figure 5.5. Maximum E_{chem} is around 6.5 eV for C, 3.5 eV for H.

Figure 5.6 shows the energy band structures of equally space pure Au, HOPT, COPT and HMAOPT structures. In chapter 4, it is pointed out that in linear pure Au wire, there is a single bond crossing the Fermi level. Due to *d* bands locating near the Fermi level, there are high density of states at Fermi level. In HOPT structures, these *d* bands are shifted down in energy away from the Fermi

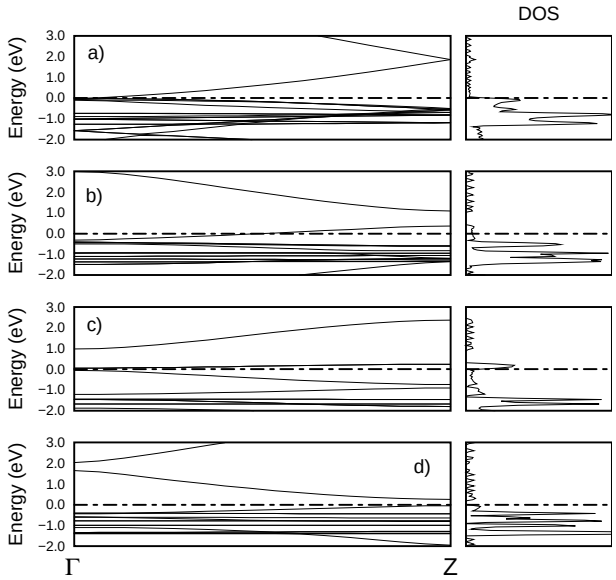

Figure 5.6: Energy band structure of pure Au in (a), HOPT in (b), COPT in (c) and HMAOPT in (d) wires. Zero of energy is taken at Fermi level. In pure Au wire, four atom supercell is used for comparison.

level, since the H state is pinned at Fermi level. A single band crossing the Fermi level at a k value is around 0.25. In COPT wire, d bands are far from below the Fermi level. But there is a small band gap (0.16 eV) near the Γ point. A band gap is also observed in HMAOPT structure (0.3 eV).

Figures 5.7 to 5.10 show the whether there is a difference between finite and infinite chains or not. It is seen that there is small differences in bond lengths when one compare the finite and infinite equilibrium structures. Au-impurity bond length is affected in a small amount when one increase the number of Au atom in finite chains. Effect of tips on bond lengths and interaction are also shown in Figure 5.10. It is seen that effect of tip on bond lengths is very small. When tip atoms are removed and wire transform the infinite linear wire, bond lengths in this infinite wire are very close the bond lengths in system having tip. It is seen from Figure 5.10 that wire tends to break the bond away from the impurity as in the case of infinite linear wire. Interaction energies are also very similar to each other.

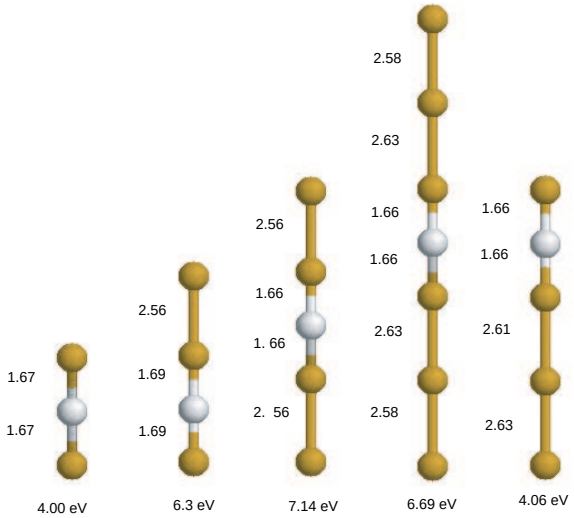

Figure 5.7: Comparison of finite and infinite wires with H. Last figure is infinite wire.

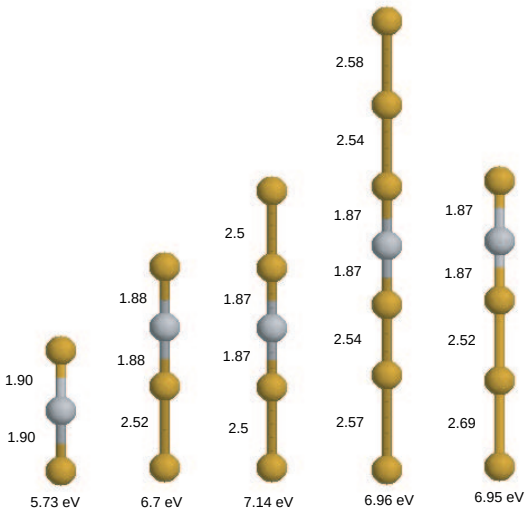

Figure 5.8: Comparison of finite and infinite wires with C. Last figure is infinite wire.

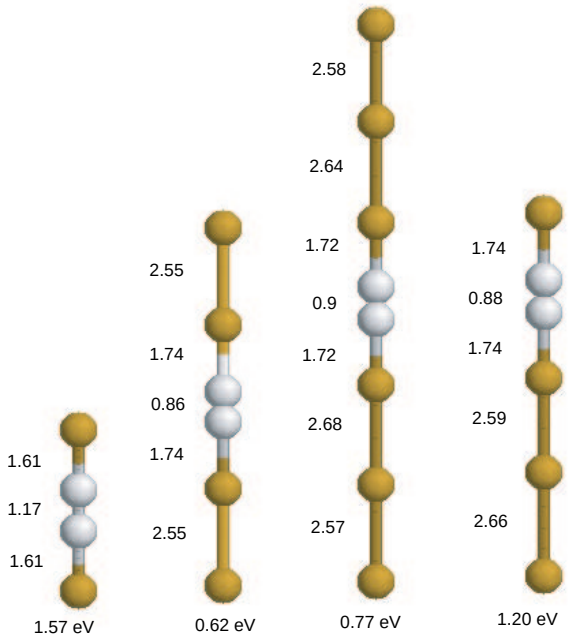

Figure 5.9: Comparison of finite and infinite wires with H_2. Last figure is infinite wire.

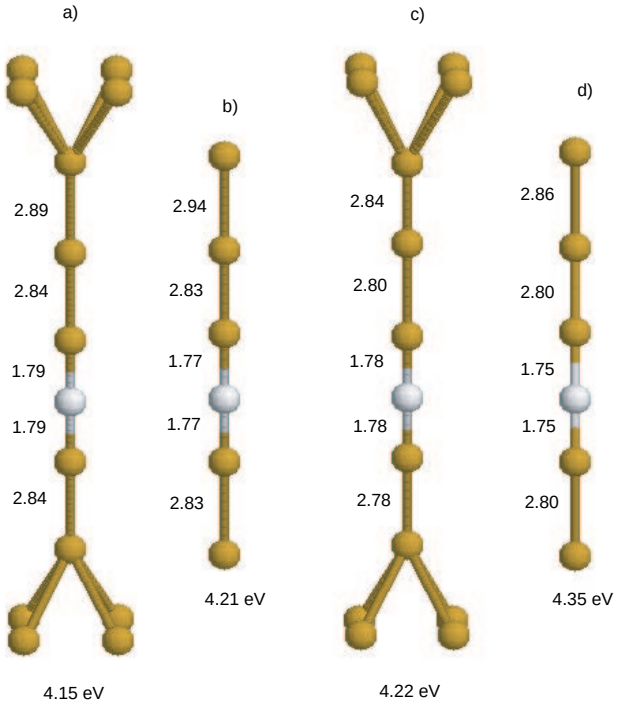

Figure 5.10: Effect of tip on bond lengths and interaction energy. In (a) lattice constant along the chain direction is 19.41 Å. In (b) tip atoms are removed and all other atoms are allowed to relax. In (c) lattice constant is 19.198 Å. In (d) tip atoms are removed and total system is allowed to relax. Energy below the figures show the interaction energy of Au chain and H.

Chapter 6

CONCLUSIONS

In the first part of the thesis, linear and zigzag structure of monatomic chains are investigated for Au, Al, Ag, Cu, Pt and Na. Au, Pt and Al have two minima in zigzag structure. All the global minima in zigzag structure have roughly the same bond angle which is slightly less than 60^o. Zigzag structure is energetically more favorable than linear structure in all elements under study. Breaking of linear chains are also studied. After a certain bond length is reached, breaking is more favorable. Breaking force for each element having linear wire geometry is calculated at breaking point. Au and Pt have the biggest breaking force. When wire break, energy curve with respect to lattice constant begins to flat. Bond energies of broken bond are calculated by using equilibrium energies and energies at which energy curve begins to become break. All the chains in both linear and zigzag structure are metallic and number of band crossing the Fermi level depend on the valence electronic structure of metal atom. The investigation of charge density contour plot gives the clue about stability of different chains of atoms relative to each other. Au, Pt, Cu and Ag have non-directional bonding. However Al and Na have directional bonding due to p orbital. In global minima of Au, Pt and Al zigzag wires, bonding becomes significant between second nearest neighbor.

In the second part of the thesis, effects of H, C and H_2 impurities on mechanical stability and electronic properties of Au wire are investigated. In a chain with C

impurity, when one applies a tension, bond far away from the C stretches much more than other two structures. C part is very rigid. However, in a chain with H, bonds stretch together. In these two structures, origin of stability is the charge transfer from Au to H and C. C affects also the second nearest neighbor. In contrast to these chains, chains with H_2 are not stable relative to others. When C and H_2 enter the chain, a gap opens around Fermi level. However, chains with H impurity are still metallic.

Bibliography

[1] H. Ohnishi, Y. Kondo and K. Takayanagi, *Quantized conductance through individual rows of suspended gold atoms,* Nature **395**, 780-785 (1998).

[2] A. I. Yanson, G. R. Bollinger, H. E. van der Brom, N. Agrait, and J. M. van Ruitenbeek, *Formation and manipulation of a metallic wire of single gold atoms,* Nature **395**, 783-785 (1998)

[3] J. C. Inkson, *Many-body theory of solids,* Plenum press, (1986).

[4] P. Hohenberg, and W. Kohn, *Inhomogeneous Electron Gas,* Phys. Rev **136**, B864 (1964).

[5] W. Kohn, and L. J. Sham *Self-Consistent Equations Including Exchange and Correlation Effects,* Phys. Rev **140**, A1133 (1965).

[6] D. Sanchez-Portal, E. Artacho, J. Junquera, P. Ordejon, A. Garcia and J. M. Soler, *Stiff monatomic gold wires with a spinning zigzag geometry,* Phys. Rev. Lett. **83**, 3884 (1998).

[7] D. Sanchez-Portal, E. Artacho, J. Junquera, A. Garcia and J. M. Soler, *Zigzag equilibrium structure in monatomic wires,* Surface Science **482-485**, 1261-1265 (2001).

[8] H. Koizuma, Y. Oshima, Y. Kondo and K. Takayanagi, *Quantitave high-resolution microscopy on a suspended chain of gold atoms,* Ultramicroscopy **88**, 17-24 (2001).

[9] H. Hakkinen, R. N. Batnett, and U. Landman, *Gold nanowires and their chemical modifications,* J. Phys. Chem. B **103**, 8814-8816 (1999).

[10] S. R. Bahn, N. Lopez, J. K. Norskov, and K. W. Jacobsen, *Adsorption-induced restructring of gold nanochains,* Phys. Rev B **66**, 081405 (2001).

[11] S. B. Legoas, D. S. Galvao, V. Rodrigues, and D. Ugarte, *Origion of anomalously interatomic distance in suspended gold chains,* Phys. Rev. Lett. **88**, 076105 (2002).

[12] N. V. Skorodumova, and S. I. Simak, *Stability of gold nanowires at large Au-Au separations,* Phys. Rev. B **67**, 121404 (2003).

[13] F. D. Novaes, A. J. R. da Silva, E. Z. da Silva, and A. Fazzio, *Effect of impurity in the large Au-Au distance in gold nanowires,* Phys. Rev. Lett. **90**, 036101 (2003).

[14] V. Rodrigues, and D. Ugarte, *Real-time imaging of atomistic process in one-atom thick metal junction,* Phys. Rev. B **63**, 073405 (2001).

[15] Y. Takai, T. Kawasaki, Y. Kimura, T. Ikuta, and R. Shimizu, *Dynamic observation of an atom-sized gold wire by phase elctron microscopy,* Phys. Rev. Lett. **87**, 106105 (2001).

[16] T. Kizuka, S. Umehara, and S. Fujisawa, *Metal-insulator transition in stable one-dimensional arrangments of sinle gold atoms,* Jpn. J. Appl. Phys. **40**, L71-L74 (2001).

[17] O. Yu. Kolesnychenko, O. I. Shklyarevskii, and H. avn Kempen, *Giant influence of adsorbed helium on field emission resonance measurement,* Phys. Rev. Lett. **83**, 2242 (1999).

[18] C. Untiedt, A. I. Yanson, R. Grande, G. Rubio-Bolliger, N. Agrait, S. Vieria, and J.M. van Ruitenbeek *Calibration of the lenght of a chain of single gold atoms,* Phys. Rev. B **66**, 085418 (2002).

[19] E.Z. da Silva, A. J. R. da Silva, and A. Fazzio, *How do gold nanowires break?,* Phys. Rev. Lett. **87**, 256102 (2001).

[20] M. Okamoto, K. Takayanagi, *Structure and conductance of a gold atomic chains,* Phys. Rev. B **60**, 7808 (1999).

[21] L. De Maria, and M. Springborg, *Electronic structure and dimerization of a single monatomic gold chain,* Chem. Phys. Lett. **323**, 293-299 (2000).

[22] J. A. Torres, E. Tosatti, A. Dal Corso, F. Ercolessi, J. J. Kohanoff, F. D. Di Tolla, J. M. Soler, *The puzzling stability of moatomic gold wires,* Surface Science **426**, L441-L446 (1999).

[23] G. Rubio-Bolliger, S. R. Bahn, N. Agrait, K. W. Jacobsen, and S. Vieria, *Mechanical properties and formation mechanism of a wire of single gold atoms,* Phys. Rev. Lett. **87**, 026101 (2001).

[24] H. Hakkinen, R. N. Batnett, A. G. Scherbakov, and U. Landman, *Nanowires gold chains: mechanism and conductance,* J. Phys. Chem. B **104**, 9063-9066 (2000).

[25] S. R. Bahn, and K. W. Jacobsen, *Chain formation of metal atoms,* Phys. Rev. Lett. **87**, 266101 (2001).

[26] J. Nakamura, N. Kobayashi, and M. Aono, *Electronic states and structural stability of gold nanowires,* Riken Rev. **37**, 17 (2001).

[27] A. Sutton, *Electronic structure of metarials,* Oxford Science Publications, (1993).

[28] I. P. Batra, *Gapless Peierls transition,* Phys. Rev. B **42**, 9162 (1990).

[29] N. V. Skorodumova, and S. I. Simak, *Spatial configuration of monatomic gold chains,* Comp. Mater. Sci. **17**, 178-171 (2000).

[30] R. H. M. Smit, C. Untiedt, A. I. Yanson, and J. M. van Ruitenberk, *Common origin for surface reconstruction and the formation of chain of metals atoms,* Phys. Rev. Lett **87**, 266102 (2001).

[31] G. Kresse, and J. Hafner, *Ab initio molecular dynamics for liquid metals,* Phys. Rev B **47**, R558 (1993).

[32] J. P. Perdew, J. A. Chevary, S. H. Vosko, K. A. Jackson, M. R. Pederson, D. J. Singh, and C. Fiolhais, *Atoms, molecules, solids, and surfaces:*

Applications of the generalized gradient approximation for exchange and correlation, Phys. Rev B **46**, 6671 (1992).

[33] D. Vanderbilt, *Soft self-consistent pseudopotentials in a generalized eigenvalue formalism,* Phys. Rev B **41**, 7892 (1990).

[34] M. C. Payne, M. P. Teter, D. C. Allan, T. A. Arias and J. D. Joannopoulos *Iterative minimization techniques for ab initio total-energy calculations: molecular dynamics and conjugate gradients* Rev. Mod. Phys. **64**, 1045 (1992).

[35] H. J. Monkhorst, and J. D. Pack, *Special points for Brillouin-zone integrations,* Phys. Rev B **13**, 5188 (1976).

[36] P. Sen, O. Gulseren, T. Yildirim, I. P. Batra, and S. Ciraci, *Pentagonal nanowires: A first-principle study of the atomic and electronic structure,* Phys. Rev. B **64**, 235433 (2002).

[37] P. Sen, S. Ciraci, A. Buldum, and I. P. Batra, *Structure of aluminum atomic chains,* Phys. Rev. B **64**, 195420 (2001).

[38] M. Sprinborg, and P. Sarkar, *Structural and electronic properties of thin chains of Ag,* Phys. Rev. B **68**, 045430 (2003).

[39] F. Ribeiro and M. Cohen , *Ab initio pseudopotential calculations of infinite monatomic chains of Au, Al, Ag, Pd, Rh, and Ru* , Phys. Rev. B **68**, 035423 (2003).

[40] T. Ono, K. Hirose, *First-principle study of Peierls instability in infinite single row Al wires,* Phys. Rev. B **68**, 045409 (2003).

[41] A. Ayuela, H. Raebiger, M. J. Puska, and R. M. Nieminem, *Spontaneous magnetization of aliminum nanowires deposited on the NaCl(100) surface,* Phys. Rev. B **66**, 035417 (2002).

[42] T. Nautiyal, S. J. Youn, and K. S. Kim, *Effect of dimensionality on the electronic structure of Cu, Ag and Au,* Phys. Rev. B **68**, 033407 (2003).

[43] W. T. Geng, and K. S. Kim, *Linear monatomic wires stabilized by alloying: Ab initio density functional calculations*, Phys. Rev. B **67**, 233403 (2003).